AD-A112 595 ROME AIR DEVELOPMENT CENTER GRIFFISS AFB NY F/G 20/14
MILLIMETER WAVE SCATTER AND ATTENUATION MEASUREMENTS ON SNOW SL--ETC(U)
SEP 81 U H LAMMERS, D T HAYES, R A MARR
UNCLASSIFIED RADC-TR-81-88 NL

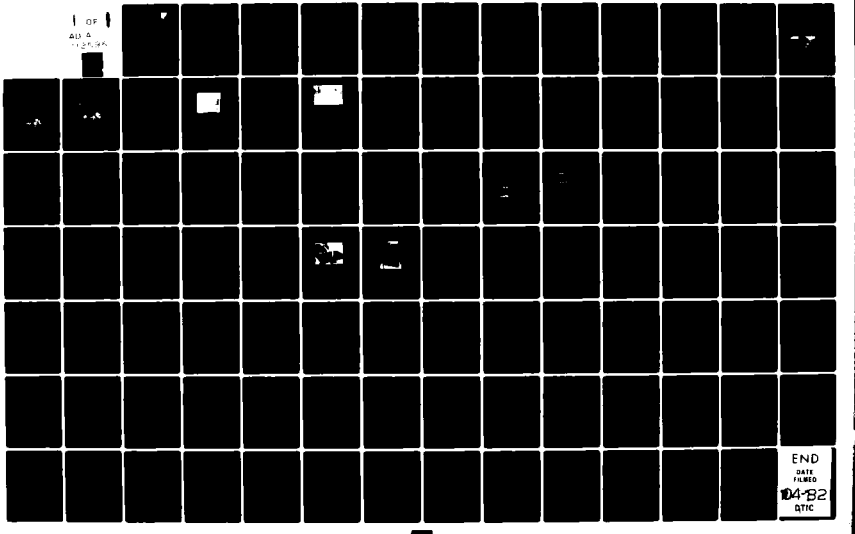

END
DATE FILMED
04-82
DTIC

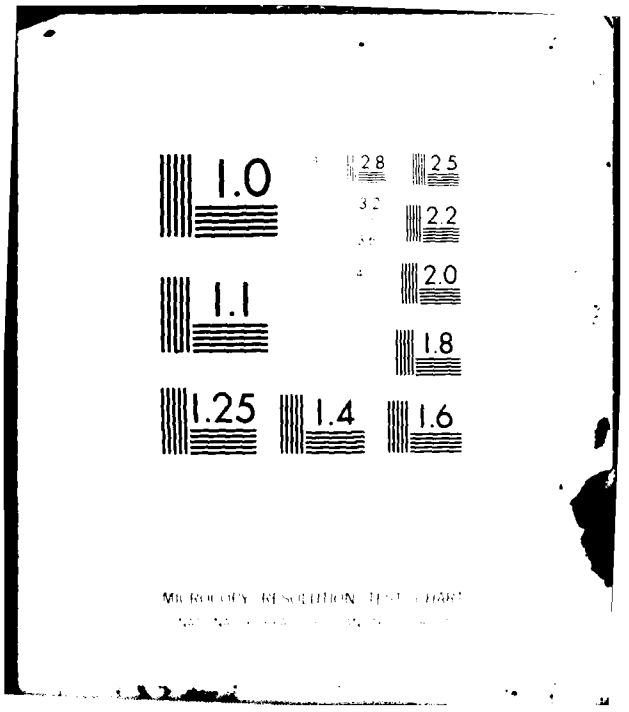
1.0
2.8
2.5
3.2
2.2
3.6
2.0
4
1.8
1.1
1.25
1.4
1.6

(12)

AD A112565

RADC-TR-81-88
In-House Report
September 1981

MILLIMETER WAVE SCATTER AND ATTENUATION MEASUREMENTS ON SNOW SLABS

Uve H.W. Lammers
Dallas T. Hayes
Richard A. Marr

APPROVED FOR PUBLIC RELEASE; DISTRIBUTION UNLIMITED

DTIC
ELECTE
MAR 29 1982
B

ROME AIR DEVELOPMENT CENTER
Air Force Systems Command
Griffiss Air Force Base, New York 13441

DTIC FILE COPY

This report has been reviewed by the RADC Public Affairs Office (PA) and is releasable to the National Technical Information Service (NTIS). At NTIS it will be releasable to the general public, including foreign nations.

RADC-TR-81-88 has been reviewed and is approved for publication.

APPROVED: Terence J. Elkins

TERENCE J. ELKINS
Chief, Propagation Branch
Electromagnetic Sciences Division

APPROVED: Allan C. Schell

ALLAN C. SCHELL, Chief
Electromagnetic Sciences Division

FOR THE COMMANDER: John P. Huss

JOHN P. HUSS
Acting Chief, Plans Office

If your address has changed or if you wish to be removed from the RADC mailing list, or if the addressee is no longer employed by your organization, please notify RADC (EEP), Hanscom AFB MA 01731. This will assist us in maintaining a current mailing list.

Do not return this copy. Retain or destroy.

Unclassified

SECURITY CLASSIFICATION OF THIS PAGE (When Data Entered)

REPORT DOCUMENTATION PAGE		READ INSTRUCTIONS BEFORE COMPLETING FORM
1. REPORT NUMBER RADC-TR-81-88	2. GOVT ACCESSION NO. AD-A112 595	3. RECIPIENT'S CATALOG NUMBER
4. TITLE (and Subtitle) MILLIMETER WAVE SCATTER AND ATTENUATION MEASUREMENTS ON SNOW SLABS		5. TYPE OF REPORT & PERIOD COVERED In-house 6. PERFORMING ORG. REPORT NUMBER
7. AUTHOR(s) Uve H.W. Lammers Dallas T. Hayes Richard A. Marr		8. CONTRACT OR GRANT NUMBER(s)
9. PERFORMING ORGANIZATION NAME AND ADDRESS Deputy for Electronic Technology (RADC/EEP) Hanscom AFB Massachusetts 01731		10. PROGRAM ELEMENT, PROJECT, TASK AREA & WORK UNIT NUMBERS 2305J603
11. CONTROLLING OFFICE NAME AND ADDRESS Deputy for Electronic Technology (RADC/EEP) Hanscom AFB Massachusetts 01731		12. REPORT DATE September 1981 13. NUMBER OF PAGES 95
14. MONITORING AGENCY NAME & ADDRESS(if different from Controlling Office)		15. SECURITY CLASS. (of this report) Unclassified 15a. DECLASSIFICATION/DOWNGRADING SCHEDULE

16. DISTRIBUTION STATEMENT (of this Report)

Approved for public release; distribution unlimited.

17. DISTRIBUTION STATEMENT (of the abstract entered in Block 20, if different from Report)

18. SUPPLEMENTARY NOTES

19. KEY WORDS (Continue on reverse side if necessary and identify by block number)
Millimeter wave propagation
Terrain scatter
Snow cover
Backscatter
Attenuation

20. ABSTRACT (Continue on reverse side if necessary and identify by block number)

During the winter of 1977/78 RADC conducted a measurement program on the backscatter, bistatic scatter, and attenuation properties of metamorphic snow at millimeter wavelengths. After going through an aging process, snow cover on the ground develops sufficient internal strength so that slabs can be cut from it and removed for measurement. Low-power CW equipment was designed and constructed to conduct scatter and attenuation measurements on snow slabs at frequencies of 35, 98, and 140 GHz at vertical, horizontal and crossed polarizations. Data were obtained as a function of the grazing angle

DD FORM 1 JAN 73 1473

Unclassified

SECURITY CLASSIFICATION OF THIS PAGE (When Data Entered)

20. (Cont)

on snow, respectively the penetration angle through snow by rotating the slab relative to the fixed-pointing transmit and receive antennas. Angles ranged from 90 deg (perpendicular incidence) to 10 deg. The major types of snow classified and measured were: (a) snow generated by melt-freeze (MF) metamorphism, (b) snow generated by equitemperature (ET) metamorphism, and (c) sleet. The snow types happened to be associated with specific periods during the winter season in the Boston area. The measurement technique does not lend itself readily to wet snow. Data reported here are strictly for frozen snow. At 35 GHz, like-polarized backscatter coefficients were found to range from 11 dB at 90 deg grazing angle to -14 dB at 15 deg with a drop-off suggesting that a coherent specular scatter mechanism contributed to the higher value. At 98 and 140 GHz, an angular dependence more typical of incoherent rough-surface or volume scatter prevailed, with backscatter coefficients only slightly lower at 90 deg grazing angle, but up between 0.5 and -6 dB at 15 deg. No clear difference was found between vertical and horizontal-polarization data. Cross-polarized backscatter was on the order of 20 dB down from the like-polarized level at 35 GHz, consistent with the specular nature of the signal. At 98 and 140 GHz, the difference was only 2 to 5 dB. Attenuation coefficients at the two higher frequencies were in the range of 300 to 500 dB/m but a factor 10 lower at 35 GHz. This led to the conclusion that a slab thickness of 12.7 cm or less as used for measurement was enough only at 98 and 140 GHz to represent conditions of very deep snow on the ground.

Preface

The support provided by Mr. J.T. Doherty and Capt. J.J. McNally during the design and measurement phases of this program is gratefully acknowledged.

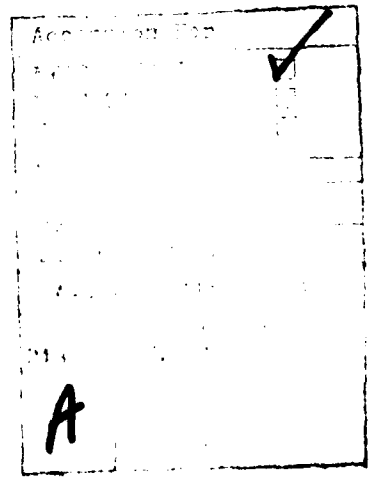

Contents

1. INTRODUCTION 9

2. SCOPE OF MEASUREMENT PROGRAM 10

   2.1 The Scatterometer-Transmissometer 11
   2.2 System Calibration 18
   2.3 Signal Characteristics 22
   2.4 Measurement Procedures and Locations 29

3. SNOW CHARACTERIZATION 30

   3.1 Snow Development 30
   3.2 Snow Measurement 32

4. EXPERIMENTAL RESULTS 33

   4.1 Sample Cases of Scatter and Attenuation 34
   4.2 Summary of Experimental Data 45
      4.2.1 Backscatter Data 46
      4.2.2 Transmission Data 54
   4.3 Comparison With Other Results 63

5. CONCLUSIONS 69

REFERENCES 73

APPENDIX A: Snow Data 75

Illustrations

1.	Snow Scatterometer, Sample Backscatter Mode	12
2.	Snow Scatterometer, Sample Bistatic Scatter Mode	13
3.	Snow Transmissometer, Sample Attenuation Mode	14
4.	Scatterometer Block Diagram	15
5.	Closeup View of Transmitters	16
6.	Closeup View of Single Receiver Frontend	18
7.	Image Source Calibration Method	19
8.	Comparison of RF and IF Calibration	22
9.	Signal Path Geometries, (a) Bistatic Scatter, (b) Reflection, (c) Attenuation	24
10.	Diagram to Compute Signal Phasing Rates	25
11.	Angular Dependence of Backscattered Power	28
12.	Sample Backscatter and Attenuation Data of 17 January 1978, (vertical polarization)	35
13.	Sample Backscatter and Attenuation Data of 28 January 1978, (vertical polarization)	36
14.	Sample Backscatter Data of 23 February 1978, (horizontal and cross-polarization)	37
15.	Sample Bistatic Scatter and Attenuation Data of 23 February 1978, (horizontal polarization)	38
16.	Backscatter From Flat Metal Plate at 35 GHz, (vertical polarization)	39
17.	Measured (—) and Predicted (---) Backscatter Fluctuation Rates	43
18.	Typical Smooth Sample of Equitemperature Snow, (edges were intact during tests)	46
19.	Typical Sample of Melt-Freeze Snow With Cusped Surface	47
20.	Backscatter Coefficient From Sleet, (data of 16 January 1978, vertical polarization)	48
21.	Backscatter Coefficient From Melt-Freeze Snow, (data of 24 January 1978, vertical polarization)	49
22.	Average Backscatter Coefficient From Sleet, (— data of 16 and 17 January 1978) and From Melt-Freeze Snow, (--- data of 24 January to 6 February 1978), Vertical Polarization	50
23.	Average Backscatter Coefficient From Equitemperature Snow, (data of 21 February to 2 March 1978, polarizations HH —, VV ---, HV -·-·-)	51
24.	Comparison of Backscatter Coefficient Measured off Thick and Thin Snow Slabs, (12.7 cm slab —, 2.5 cm slab ---)	53
25.	Hypothetical Attenuation Curve for Scattering Medium	57
26.	Attenuation vs Slab Thickness at 35 GHz, (polarizations vertical o, horizontal x)	61
27.	Attenuation vs Slab Thickness at 98 GHz, (polarizations vertical o, horizontal x)	61

28.	Attenuation vs Slab Thickness at 140 GHz, (polarizations vertical o, horizontal x)	62
29.	Comparison of Sample and In-situ Data at 35 GHz	64
30.	Comparison of Sample and In-situ Data at 98 GHz	65
31.	Comparison of Sample and In-situ Data at 140 GHz	66
32.	Diagram Illustrating the Stiles and Ulaby[18] Attenuation Measurement Through Layers of Snow at 35.6 GHz	67
33.	Path Loss Measured by Stiles and Ulaby[18] as a Function of Snow Thickness	67

Tables

1.	E- and H-Plane Beamwidths of Transmitting and Receiving Antennas	16
2.	Backscatter From Sample Holder	29
3.	Average Parameters of Snow Cover	39
4.	Fluctuation Characteristics of Attenuated Signal	44
5.	Average Attenuation Coefficient, (vertical polarization, 17 January to 2 February 1978)	58
6.	Average Attenuation Coefficient, (vertical and horizontal polarization, 21 February to 2 March 1978)	59
7.	Calculated Attenuation Coefficient of Snow Using Wiener Formula	60
8.	Attenuation Coefficient vs Frequency, (initial slope of curves fitted to data)	62
9.	Loss Measurements at 35 GHz and 95 GHz by Currie et al[7]	68
10.	Loss Caused by Snow and Ice at 35 GHz, (Battles and Crane[23])	69
A1. thru A20.	Physical Parameters of Snow Cover	76 thru 95

Millimeter Wave Scatter and Attenuation Measurements on Snow Slabs

1. INTRODUCTION

Millimeter wave component technology has advanced to a state where a large number of military system applications are coming under consideration. The advantages of small size, high antenna-beam resolution, and large bandwidth are widely recognized, particularly onboard space-limited aircraft and missiles. Propagation phenomena such as high attenuation in the molecular resonance bands and in heavy precipitation are not a problem in many tactical applications. In fact, covertness beyond the intended operational range is considered an advantage in many cases. Imaging, ranging, and homing millimeter wave sensors interact with natural backgrounds. It has been found that old granular snow covering the ground can have unusually strong reflective properties at millimeter wavelengths. The implications of a high reflectivity of metamorphic snow must be of concern to military-system designers.

A recent survey by Suits and Guenther[1] on the scattering of natural backgrounds in the millimeter wave region showed only limited data in the present literature. Measurements at shorter wavelengths, on old granular snow in particular, are scarce or non-existent. A further drawback on snow measurements quite often is

(Received for publication 17 September 1981)

1. Suits, G. H., and Guenther, B. D. (1978) Targets and Backgrounds, U.S. Army MIRADCOM, Tech. Rep. T-78-71.

the lack of an adequate description of the meteorological conditions and snow composition under which the scatter data were obtained.

The University of Kansas[2] has reported on snow backscatter measurements, conducted in the winter of 1975 over the frequency range 1 to 18 GHz. During February and March of 1977 further measurements[3,4] of snow backscatter in Colorado extended the frequency range to include 1 to 18 GHz and 35 GHz. Data were acquired at numerous frequencies, polarizations, and grazing angles for a variety of carefully observed snow conditions. Ellerbruch et al[5] at the National Bureau of Standards have used frequencies between 0.5 and 18 GHz to probe the stratigraphy of snow based on backscatter techniques. Antennas mounted directly above the snow detected reflections from depths up to 4 m depending on frequency. Hoekstra and Spanogle[6] determined the scattering from snow in New Hampshire at low grazing angles for 10 and 35 GHz. Prompted by earlier Honeywell findings of snow effects on experimental millimeter wave sensors, the Georgia Institute of Technology conducted measurements[7,8] at 35 and 95 GHz, again in Colorado during the later winter of 1975/76. Despite limitations in the experiment, evidence was found of some of the peculiarities of metamorphic snow at millimeter wavelengths: its ability to produce strong scattering in the frozen state, the existence of changes in reflectivity associated with the diurnal melt-freeze cycle, and the high attenuation of signals passing through snow, suggesting that scattering is a near-surface effect. Ulaby et al[9] have published a state-of-the-art review of the microwave backscatter and emission behavior of snow. Trebits et al[10] in another review of millimeter wave background scatter compare snow data obtained by the University of Kansas and the Georgia Institute of Technology. They point out that a substantial increase in snow reflectivity has been observed when going from 10 to 35 GHz.

In order to better understand these phenomena, and to obtain quantitative data at 35, 98, and 140 GHz, the Propagation Branch at RADC has conducted a measurement program during the winter of 1977/78 and investigated backscatter, bistatic scatter, and attenuation characteristics of metamorphic snow at these frequencies.

2. SCOPE OF MEASUREMENT PROGRAM

A choice had to be made with regard to the frequencies at which to obtain data. Component technology and hence exploratory system development is most advanced in the 35-GHz region and to a slightly lesser extent in the 94-GHz region. The status of 140 GHz and higher-frequency technology must still be considered

---

(Due to the large number of references cited above, they will not be listed here. See References, page 73.)

experimental. Based on the current need to establish the tradeoffs between 35-GHz and 94-GHz systems, and a possible requirement for 140-GHz data in the near future, the determination was made to derive comparative data at these three frequencies.

In many of the prospective applications of millimeter waves, imaging of natural backgrounds or of man-made targets against natural backgrounds plays an important role. Imaging or target-to-background studies involve complexities that would distract from a study of basic millimeter-wave/snow interaction. No effort was undertaken during the present phase of the program other than the direct measurement of snow scatter and attenuation parameters.

2.1 The Scatterometer-Transmissometer

During the planning stages of the experiment it became obvious that suitable commercially developed equipment was unavailable to RADC. The decision was made to design and construct short-range scatterometers in-house which would permit the measurement of backscatter coefficients and bistatic scatter coefficients as well as attenuation coefficients on samples of metamorphic snow, removed from natural snow surfaces. In later stages of metamorphism, this can be accomplished without disturbing the snow in a noticeable way. The main objectives in the equipment design were: (a) flexibility in measuring a wide range of propagation parameters on snow, (b) ruggedness for operation in the field, and (c) the use of components available in-house to accelerate equipment construction in order to perform measurements during the winter 1977/78.

Standard gain horn antennas for transmission and reception at the three frequencies permit far-field measurements at ranges of 1 m with 3-dB beam diameters of approximately 0.24 m. This, combined with the fact that old granular snow has sufficient rigidity to permit the removal of large frozen slabs from the ground, led to the development of a sample measurement technique incorporated in the equipment shown in Figure 1. A sled-like platform was constructed from plywood with metal-underlaid runners to permit easy movement on snow. A double wooden boom is rigidly attached to the platform, extending upward at 45 deg. At its upper end, this boom carries a wooden basket to hold a snow sample of 0.76 m length and 0.56 m width. The sample holder rotates around a horizontal axis. A double wooden boom extension pivots around the same axis. On the end crossmember of the boom extension the receivers are mounted. The transmitters are located on a crossmember at the lower end of the rigid boom near the sled platform. Both the transmitting and receiving antennas are pointing at the common axis of rotation and hence at the center of the snow sample. This is independent of the angular position of the snow surface relative to the transmitter and receiver antenna directions. In

the configuration shown, the transmitter-target-receiver geometry approaches that for backscatter. The maximum angle between transmitted and scattered signal directions is 170 deg with transmitting and receiving antennas almost touching each other. The snow sample in the basket is inverted from its natural position and is prevented from falling out by a woven net of waxed string or nylon fishing line. A major advantage of this design results from the fact that for the backscatter and most bistatic scatter geometries the antennas are directed toward space. The necessary support structures are made of wood, again minimizing unwanted scatter signals. Other advantages of the design include the ease and repeatability with which specific scatter geometries can be configured and also transmission measurements through snow be made.

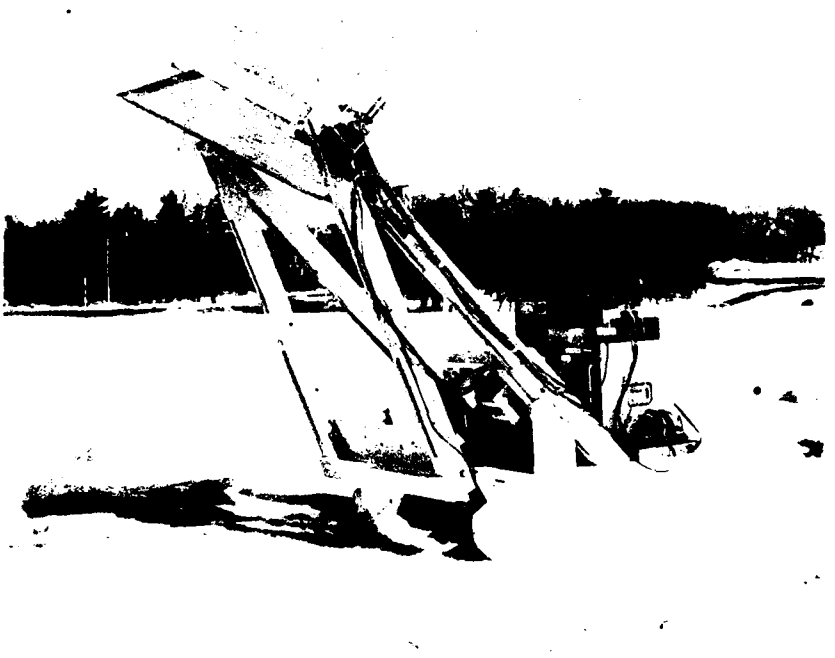

Figure 1. Snow Scatterometer, Sample Backscatter Mode

The transmitter and receiver antenna beams, pointing toward the axis of rotation of the sample holder, were fixed for the duration of a scan, during which the snow sample was slowly rotated by a motor and gear drive. This resulted in a

range of grazing angles on the snow slab, limited in the backscatter mode on one end by the length of the antenna "footprint" exceeding the length of the slab. On the other end, the basket was stopped at a near-vertical orientation, beyond which the snow slab is in danger of falling out.

In the bistatic scatter mode (Figure 2), the scatter angle between the transmitted and received beams is reduced by swinging the upper portion of the boom away from its tucked-in position in Figure 1. The minimum usable scatter angle is reached when the transmitting antenna footprint matches the snow slab in length and the receiving antenna intercepts a signal reradiated nearly tangentially from the snow surface. Under these conditions, the transmitter and receiver beam angles, measured relative to the surface of the snow, are unequal. In order to obtain a useful scan range in the bistatic mode, the scattering angle must be larger than the minimum. In general, it is chosen large enough so that the case of equal transmitter and receiver beam angles is included in the scan. From an applications viewpoint, unequal angles are possible and therefore of interest. During a scan, the angle between the boom sections is constant while the basket rotates. This means that transmitter and receiver beam angles change in opposite directions with their sum (the scatter angle) held constant.

Figure 2. Snow Scatterometer, Sample Bistatic Scatter Mode

Figure 3 shows the equipment set up as a transmissometer. In this configuration the upper half of the boom is extended into a straight line with the lower half. The signal transmitted at the lower end of the boom, penetrates the snow slab. The energy that is received by the receiver at the outer end of the boom, determines how the equipment permits the angular scan, attenuation was not simply measured by placing the snow slab in a position perpendicular with the transmitter-receiver axis but was determined as a function of snow slab angular position relative to the transmitting wave.

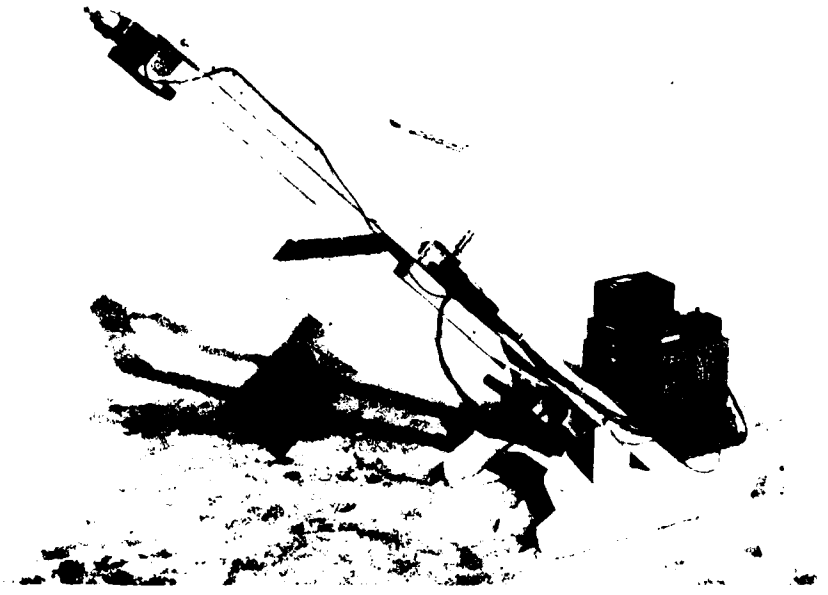

Figure 3. Snow Transmissometer, Simple Attenuation Mode

Several problems exist with the sample measurement technique. One is the difficulty in picking up snow in relatively early stages of melt, perhaps when it is only an ice crust, when it is still brittle and incapable of supporting itself over sufficiently large areas. A certain skill was acquired during the measurement to handle breakable snow slabs by supporting them with a metal plate until firmly placed in the basket. With snow containing a percentage of liquid water, the inverted orientation could lead to incorrect measurement, if sufficient water is present to

establish a flow. Subsequently, this would lead to a concentration of water near the surface. Measurements in the sample mode were generally confined to frozen metamorphic snow slabs, the type that gives rise to the most severe reflections on the ground.

In Figure 4 a simplified diagram presents the basic transmitter and receiver building blocks and a schematic view of antenna and basket arrangement. There are three individual transmitters mounted side by side on an adjustable board between the members of the boom. The transmitters, as is seen in Figure 5, consist of microwave sources and horn antennas. They can be rotated about their longitudinal axes, to permit transmission at vertical and horizontal polarization.

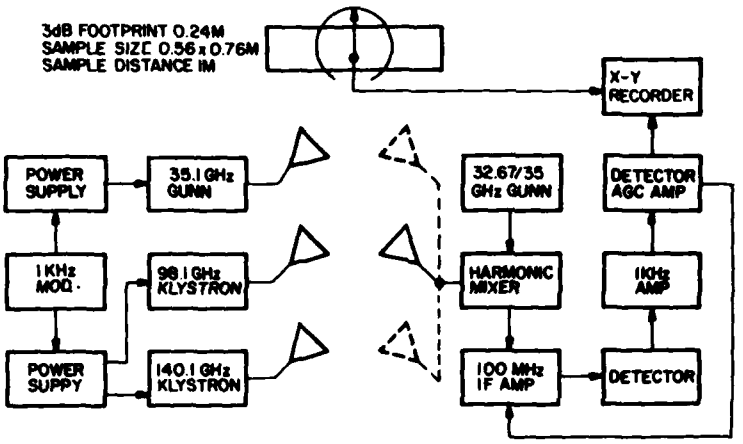

Figure 4. Scatterometer Block Diagram

Klystron oscillators (VC 710C and VRT 2123A) are used at 98 and 140 GHz. A Gunn oscillator (VSA 9010EW) serves as the 35-GHz source. Power output at all frequencies is of the order of 1 mW. The klystrons were operated at the lowest beam voltage (1500 V) at which oscillations were reliably sustained. Sufficient dynamic range for snow slab measurements was obtained with reduced power output. Lower input power improved both frequency stability and reliability of the mm-wave tubes. The transmitters are powered by separate power supplies (Figure 4) and are on/off modulated by a common squarewave modulator at a 1-kHz rate. The transmitters use standard gain horn antennas at 35 and 98 GHz and a scalar feed horn at 140 GHz. The footprint on the snow slab at perpendicular orientation (approximately 0. 24 m in diameter between the 3-dB points of the individual beam pattern)

is well contained within the slab area of 0.56 × 0.76 m. Beamwidths of transmitting and receiving antennas are listed in Table 1.

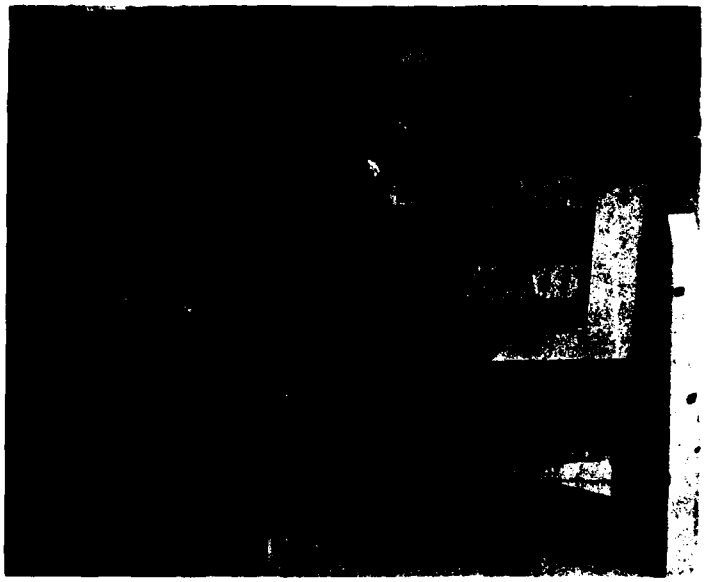

Figure 5. Closeup View of Transmitters

Table 1. E- and H-Plane Beamwidths of Transmitting and Receiving Antennas

Frequency (GHz)	Transmitting Antenna Calc. 3-dB Beamwidth		Receiving Antenna Calc. 3-dB Beamwidth	
	β_E (deg)	β_H (deg)	β_E (deg)	β_H (deg)
35	9.1	6.8	13.9	11.8
98	9.3	7.0	12.1	9.9
140	7.2	7.2	8.5	7.0

Based on microwave components available and the goal to keep the equipment as simple as possible, a single heterodyning receiver was designed. The three frequencies are received in a modified K_a-band waveguide mixer (TRG A965 with Schottky barrier diode) and downconverted to IF frequency by either using the local

oscillator (L. O.) fundamental frequency or its third or fourth harmonic. The choice of 98 GHz rather than the center frequency of that atmospheric transmission window is explained by the need to tune a single local oscillator to within IF range of the three transmitted frequencies. The relative insensitivity to frequency of the scattering and attenuation effects observed with this equipment justifies the receiver design. The specific Gunn oscillator used here (Varian VSA 9010EW) was found to tune satisfactorily over a frequency range from 32.67 to 35.0 GHz, substantially exceeding its specified tuning range. With 100 MHz the IF center frequency, the following exact frequency combinations were used: (a) transmit frequency 140.1 GHz, L.O. Frequency 140.0 GHz or fourth harmonic of 35.0 GHz, (b) transmit frequency 98.1 GHz, L.O. frequency 98.0 GHz or third harmonic of 32.67 GHz, and (c) transmit frequency of 35.1 GHz, L.O. frequency 35.0 GHz. An intermediate frequency bandwidth of 20 MHz generally accommodates oscillator drift associated with temperature changes in the outdoor environment. A picture of the receiver frontend is shown in Figure 6. The unit is mounted on an adjustable board at the outer end of the boom extension. As a unit, the receiver frontend can be rotated by 90 deg around its antenna-mixer axis to receive signals of either vertical or horizontal polarization. It can also be mounted in three laterally displaced positions for proper lineup with each transmitter antenna. A standard M-band gain horn with an M/K_a-band transition as shown in Figure 6 is used for reception at both 98 and 140 GHz. At the higher frequency the waveguide is oversized. The receiver beam pattern at 140 GHz was measured and found to agree with that calculated in Table 1. A standard K_a-band gain horn is used to receive the 35-GHz signal.

The receiver frontend consists of the antenna, mixer, L.O., bias supply, and a 35-dB IF preamplifier. The remainder of the receiver, mounted on the back of the sled, consists of components shown in the block diagram (Figure 4). Two cascaded balanced mixers (Z-MATCH DBM-100B) are connected as electronically controlled variable attenuators with a range in excess of 70 dB for automatic gain control (AGC). They are followed by another 35-dB IF amplifier. After detection, the 1-kHz squarewave modulated signal is amplified in an HP 415E Standing Wave Indicator of 15 Hz bandwidth. The rectified 1-kHz output signal drives the AGC amplifier, whose gain curve was adjusted for near-logarithmic receiver response over a 50-dB input signal range. The rectified 1-kHz signal also drives the Y-axis of a Moseley XY-recorder. The X-axis signal is a potentiometer-derived dc voltage proportional to the angular position of the snow basket. The time constant of the receiver is essentially determined by the mechanical time constant of the XY-recorder. The recording speed, that is, the speed of rotation of the equipment was empirically set so that the recording system could trace the actual signal excursions.

Figure 6. Closeup View of Single Receiver Frontend

2.2 System Calibration

Attempts were made to refer the snow scatter signals to the known return from corner reflectors or small metal plates. The results were generally not as satisfactory as those obtained with a flat metal plate large enough to exceed the size of the antenna beam cross section. The similarity of this plate to an infinite plane and the image-source concept were investigated in some detail. Signal levels were compared between the equipment configuration in Figure 3 with the sample holder empty and that of Figure 1 with a flat metal plate of 0.56 × 0.76 m filling the sample holder and the boom extension swung into the 170-deg scatter angle direction. With the plate oriented perpendicular to the line dividing the angle between the transmitter and receiver directions, signal levels during system checkout agreed to within 0.5 dB in both cases. This was found at all frequencies.

A schematic view of the image-source calibration procedure is presented in Figure 7. Two measurements are performed in sequence. First, the return from the "infinite" metal plate at range r_p from the scatterometer is determined. For the purpose of illustration, the transmitter and receiver (TX/RX) are co-located. An image transmitter TX' at twice the range r_p from the receiver leads to a power level equal to that received from the plate

$$P_{RP} = \frac{P_T \quad G_T \quad A_E}{4 \pi (2 r_p)^2} \tag{1}$$

where

P_T transmitted power,

G_T transmit antenna gain, and

A_E effective receiving aperture.

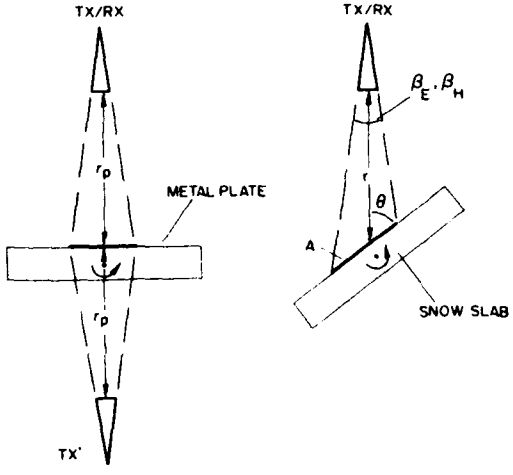

Figure 7. Image Source Calibration Method

It is assumed here that the reflecting plane is perpendicular to the beam direction as indicated in Figure 7. Second, the return from snow is determined. With the antenna beams directed at an angle θ (grazing angle) against the snow surface, the area A is illuminated by the transmitting antenna. For small β_E, β_H the area A is of elliptical shape and of size

$$A = \frac{\pi \beta_E \beta_H r^2}{4 \sin \theta} \tag{2}$$

with

β_E, β_H 3-dB E- and H-plane transmit antenna beamwidths and

r range to snow surface.

The received power from the snow becomes

$$P_R = \frac{P_T G_T \sigma^\circ A A_E}{(4\pi r^2)^2} \tag{3}$$

where σ° is the backscatter cross-section of snow per unit area.

Note that Eq. (1) describes the one-way path loss of propagation in free space, while Eq. (3) describes the incoherent radar return from a target of size A. Eq. (3) is simplified from its original integral form by assuming that G_T, σ°, and r are constant over the region A of integration. At extremely shallow angles θ this may not be a sufficiently good approximation. The backscatter coefficient σ° is obtained by combining Eqs. (1) through (3)

$$\sigma^\circ = \frac{P_R}{P_{RP}} \cdot \frac{4 \sin\theta}{\beta_E \beta_H} \cdot \left(\frac{r}{r_p}\right)^2 . \tag{4}$$

Only the received power ratio, the range ratio, the grazing angle on the snow, and the transmitting antenna beamwidths enter into the equation. The receiving antenna parameters do not affect the determination of σ°. The calibration metal plate was attached to the underside of the sample holder during the reference measurement, in order to avoid disturbing the snow sample. The minor range difference between metal and snow surfaces was accounted for in the calculation. It is assumed that most of the snow scatter occurs close to the surface.

Bistatic scatter coefficients are determined in a similar way. Ranges r to the transmitter and receiver are identical by design and the same as in the backscatter case. Two beam angles have to be considered now: θ_T between transmitted beam and snow surface, and θ_R between received beam and snow surface. Re-examining Eqs. (1) through (4) one finds that these still hold in the bistatic case if θ_T is substituted for θ. The beamwidths β_E and β_H are transmitter beamwidths as before. The bistatic scatter coefficient then becomes

$$\sigma^\circ{}_{\theta_T, \theta_R} = \frac{P_R}{P_{RP}} \frac{4 \sin\theta_T}{\beta_E \beta_H} \cdot \left(\frac{r}{r_p}\right)^2 . \tag{5}$$

The attenuation coefficient of snow may be defined from a loss measurement when the signal passes through a layer of snow. With the equipment configured as in Figure 3, power P_R is received through the snow. Rather than making a reference measurement by removing the snow slab, the backscatter reference measurement is used as in Figure 1 with the metal plate mounted under the basket. For slab thickness s we define the attenuation coefficient as

$$L = -10 \log\left(\frac{P_R}{P_{RP}}\right) \cdot s^{-1} \text{ in dB/m} . \tag{6}$$

This procedure avoids the inconvenience of removing the snow slab and the danger of breaking it in the process.

In any of the measurements, only one microwave parameter, the ratio P_R/P_{RP} of received power from the snow to received power from a reference target, is required. Transmitted power levels are of no importance and were not determined accurately. In order to establish the ratio P_R/P_{RP} in an individual measurement, the data recorded by the XY-recorder were calibrated with a precision IF calibrator (HP 355B) inserted after the first IF amplifier. The accuracy of this attenuator was checked over a 70-dB range by comparison with a calibrated signal from a signal generator (HP 608A). The deviation was less than ± 0.2 dB over the whole range. Assuming that the first conversion in the receiver is inherently linear, this would also be the accuracy expected for the received mm-wave signal. To check this assumption, measurements were made directly at 35 and 98 GHz, where 50-dB variable precision attenuators were available. The two transmitters were placed 2 m from the receiver with the variable attenuators connected between the sources and the antennas. Calibration points were obtained by comparing the receiver output level after: (a) inserting a specific attenuation into the mm-wave attenuator, and (b) replacing it with the same attenuation at IF frequency. Curves are plotted in Figure 8 of the recorder's Y-excursion as a function of the RF and IF attenuator settings. Note that two different curves are shown for the IF attenuator at 35 and 98 GHz. This can be explained in the following way. Differences in transmitted power, antenna gain, and mixer conversion loss lead to different output levels at the XY-recorder for 0-dB RF and IF attenuation. During calibration measurements, the recorder output was set to full-scale at either frequency by changing the recorder dc gain. This, in combination with the near-logarithmic receiver response, leads to different IF attenuator curves in Figure 8. Consequently, comparisons are possible only between curves taken at the same frequency.

At 35 GHz, any particular receiver output amplitude corresponds to IF and RF attenuator settings different by no more than 1 dB. When set to the same value, the RF attenuator produces an output lower than the IF attenuator with the exception of the very high attenuations, where some leakage around the RF attenuator was noticed. In contrast, at 98 GHz the RF attenuator curve is always above the IF attenuator curve, with the difference at any particular receiver output amplitude not exceeding 1 dB in the attenuation range from 0 to 30 dB and not exceeding 3 dB for the remainder of the range. Because of deviations in opposite directions at 35 and 98 GHz, it is assumed that these are basically due to RF attenuator calibration error. The absolute error is in line with the 2-percent accuracy quoted for precision RF attenuators. The increasing deviation at 98 GHz in the range between 30 and 50 dB is attributed to leakage. Leakage does not affect the snow measurements, since no RF calibration is performed there. System calibration at all frequencies, including 140 GHz, is normally achieved by variable IF attenuation.

IF attenuation is known with better accuracy, and the 35-GHz curves in Figure 8 suggest good RF to IF conversion linearity over a 50-dB range.

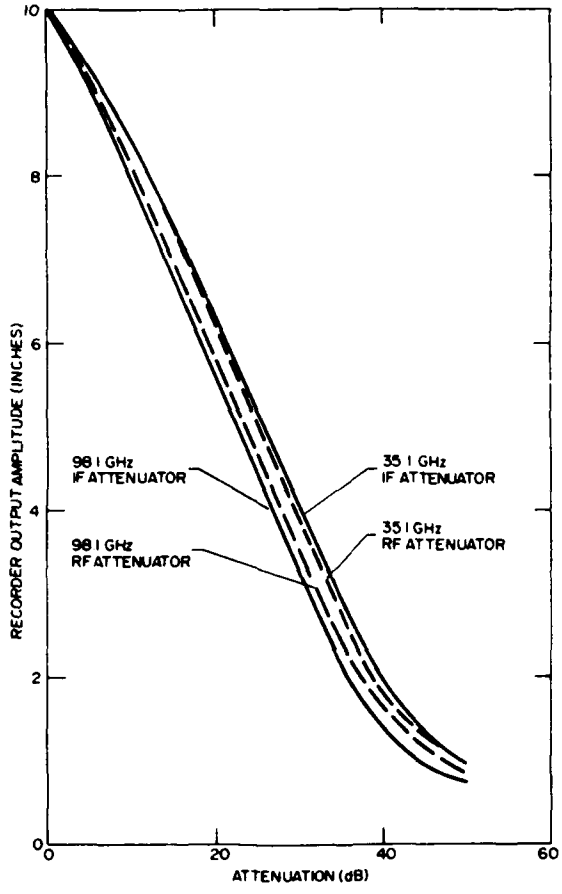

Figure 8. Comparison of RF and IF Calibration

2.3 Signal Characteristics

Frozen metamorphic snow that can be picked up for measurement consists of several discernible structures. Snow/ice pellets in various stages of transition closely packed and bonded together represent the predominant structure. Depending on the melt-freeze cycle and on rainfalls, horizontal layers appear of varying thickness. Sometimes the layers are of solid ice. The dielectric properties of ice

at 0°C have been given in a survey paper by Ray.[11] At 35, 98, and 140 GHz, the real part of the refractive index is $n_r = 1.78$. The imaginary part is $n_i = 9 \times 10^{-4}$ at 35 GHz, $n_i = 5 \times 10^{-4}$ at 98 GHz, and $n_i = 3 \times 10^{-4}$ at 140 GHz. Frozen snow is an ice-air mixture whose dielectric properties can be computed from the fractional volumes occupied by the constituents. In an earlier report,[12] we determined for freshly fallen snow $n_r^2 = 1.12$ and for late metamorphic snow $n_r^2 = 1.92$. From the low imaginary component of the refractive index, it follows that any appreciable attenuation in the medium is predominantly due to scattering. Based on a multitude of closely packed low-loss spherical scatterers, we expect to receive a Rayleigh-distributed signal of random amplitude, as the snow slab rotates relative to transmitter and receiver directions. To the extent that the ice layers are capable of specular reflection, we expect at least a fraction of the received signal to show a behavior similar to that signal reflected from the metal calibration plate.

A theoretical analysis for densely packed low-loss Mie scatterers does not exist at this time. Lacking a rigorous theory, we present somewhat qualitative models in order to explain experimentally observed signal amplitudes and fluctuation rates as a function of grazing angle θ. Consider in Figure 9(a) a bistatic system where transmitter TX and receiver RX with angular spacing θ_o and range ℓ are connected through scatterers S_1 and S_2. Both scatterers are within the snow slab, S_1 at the center of rotation and S_2 at a distance d from the center, where d is chosen to be the distance to the edge of the 3-dB transmit antenna cone. At this extreme point illuminated by the antenna and for some angular change $d\theta$ of the slab, S_2 travels the greatest distance of all scatterers within the beam and hence changes pathlength $\ell_1 + \ell_2$ the most. The change in pathlength for a signal scattered from S_2 relative to the signal from S_1 over constant path 2ℓ gives rise to a phase-shift between the two components of the received signal. There may be constructive or destructive interference. Depending on the wavelength used and other geometrical parameters, an angle change $d\theta$ can be calculated, required to change the phase angle between the two phasors from 0 to 180 deg. We determine first the rate of range change as a function of grazing angle θ. According to the law of cosines, we find from Figure 9(a)

$$\ell_1^2 = \ell^2 + d^2 - 2\,\ell d \cos(\theta + \pi - \theta_0) \text{ and}$$

$$\ell_2^2 = \ell^2 + d^2 - 2\,\ell d \cos\theta .$$

---

11. Ray, P.S. (1972) Broadband complex refractive indices of ice and water, Appl. Optics 11(No. 8):1836-1844.

12. Lammers, U.H.W., and Hayes, D.T. (1980) Multipath Propagation Over Snow at Millimeter Wavelengths, In-House Rep. RADC-TR-80-54, AD A087747.

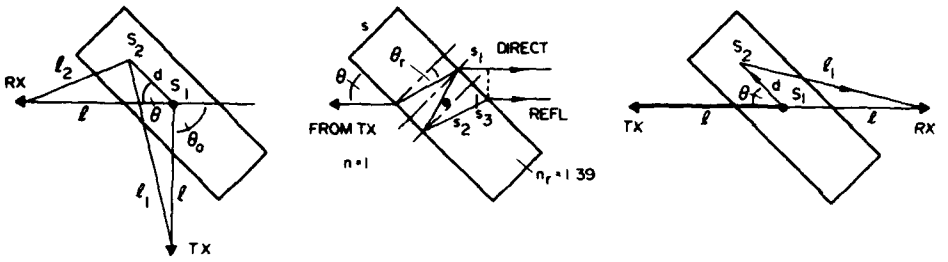

(a) (b) (c)

Figure 9. Signal Path Geometries, (a) Bistatic Scatter, (b) Reflection, (c) Attenuation

We differentiate

$$\ell_1 + \ell_2 = (\ell^2 + d^2 + 2\,\ell d \cos(\theta - \theta_0))^{1/2} + (\ell^2 + d^2 - 2\,\ell d \cos\theta)^{1/2},$$

and obtain

$$\frac{d(\ell_1 + \ell_2)}{d\theta} = \frac{\ell d \sin\theta}{(\ell^2 + d^2 - 2\,\ell d \cos\theta)^{1/2}} - \frac{\ell d \sin(\theta - \theta_0)}{(\ell^2 + d^2 + 2\,\ell d \cos(\theta - \theta_0))^{1/2}}. \tag{7}$$

The backscatter case follows from the general bistatic case by setting θ_0 to 180 deg

$$\frac{d(\ell_1 + \ell_2)}{d\theta} = \frac{2\,\ell d \sin\theta}{(\ell^2 + d^2 - 2\,\ell d \cos\theta)^{1/2}}. \tag{8}$$

The transmission case (θ_0 = 0 deg, transmitter and receiver on a straight line) yields

$$\frac{d(\ell_1 + \ell_2)}{d\theta} = \frac{\ell d \sin\theta}{(\ell^2 + d^2 - 2\,\ell d \cos\theta)^{1/2}} - \frac{\ell d \sin\theta}{(\ell^2 + d^2 + 2\,\ell d \cos\theta)^{1/2}}. \tag{9}$$

Results calculated from Eqs. (7), (8), and (9) are plotted in Figure 10 and labeled "Bistatic Scatter", "Backscatter", and "Attenuation (Single Scatter)", respectively. For grazing angles θ between 90 and 15 deg, the change in pathlength in mm/deg of slab rotation for the signal scattered at S_2 can be read from Figure 10. For each of the wavelengths (8.6 mm, 3.0 mm, and 2.1 mm) the phase change for the signal

scattered at S_2 is calculated from this value. A rough measure is obtained of how many signal fluctuations can be expected over the snow slab angular range of motion. Note that only phasing between scatterers at extreme and center points has been considered.

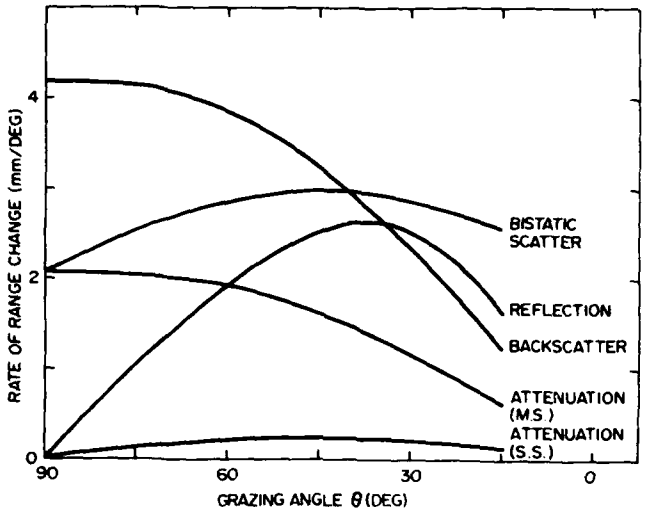

Figure 10. Diagram to Compute Signal Phasing Rates

In the backscatter case, pathlength changes of 4.2 mm at θ = 90 deg and 1.2 mm at θ = 15 deg result from a 1-deg slab rotation. This translates into a 176-deg phase change at 8.6 mm wavelength and a 720-deg phase change at 2.1 mm wavelength (both at grazing angle θ = 90 deg). Conversely, we calculate that in order to go from constructive to destructive interference at this slab orientation (phase change of 180 deg) the basket must rotate 1 deg at 8.6 mm wavelength and 0.25 deg at 2.1 mm wavelength. At a grazing angle θ = 15 deg, phase changes are about 3.5 times less per 1-deg basket rotation. Only one curve of bistatic scatter is shown in Figure 10. For θ_0 = 90 deg, the rate of range change as a function of slab angle peaks at θ = 45 deg at a level (3 mm/deg) comparable to that found for backscatter.

Experimental attenuation measurements on snow slabs frequently show substantial and rapid phasing as a function of the grazing angle. This is not surprising since scattering from low-loss dielectric spheres should produce substantial forward scatter. The curve labeled "Attenuation (Single Scatter)" gives phase differences to be expected between signals propagating along the straight transmitter/receiver path (θ = 0 deg) and that path including scatterer S_2 at radius d. When the basket is perpendicular to the straight line connecting the transmitter and the receiver, the

rate of change is zero. It reaches a maximum of 0.25 mm/deg at around θ = 45 deg. This value is much lower than the one for backscatter and does not account for the rate of phase fluctuations actually observed experimentally. In order to account for effects observed, three other interference phenomena involving the snow slab have been investigated. In the first case (depicted in Figure 9(b)) it is assumed that the homogeneous plane-parallel dielectric snow slab (n_r = 1.39) refracts and reflects the microwave signal. Interference is set up between the direct signal (refraction only) and the reflected signal (refraction and reflection). As before, a calculation of phase relationship is made. No consideration is given to the magnitude of the reflection coefficient or the losses inside the medium. According to Snell's law we write

$$\sin (90 - \theta) = n_r \sin \theta_r \text{ or } \theta_r = \frac{\cos \theta}{n_r} .$$

The path difference, which we are interested in, is

$$r = 2 s_2 - s_1 .$$

Quantity r can be expressed in terms of the slab thickness s, refractive index n_r, and angle θ shown in Figure 9(b)

$$r = \frac{2 s (1 - \cos^2 \theta / n_r)}{(1 - \cos^2 \theta / n_r^2)^{1/2}} . \tag{10}$$

Differentiation of Eq. (10) with respect to θ yields

$$\frac{dr}{d\theta} = \frac{4 s \sin \theta \cos \theta}{n_r (1 - \cos^2 \theta / n_r^2)^{1/2}} - \frac{2 s (1 - \cos^2 \theta / n_r) \sin \theta \cos \theta}{n_r^2 (1 - \cos^2 \theta / n_r^2)^{3/2}} . \tag{11}$$

This equation is also plotted in Figure 10 and labeled "Reflection". Typicall , it produces minimum phase change as the basket moves through the region where the direct signal penetrates the slab perpendicularly. We see, however, that for angles θ near 40 deg, phasing is as rapid as for the backscatter case. The maximum rate of range change in this area is 2.6 mm/deg.

Another mechanism conceivable to introduce rapid phase fluctuations into the attenuation measurement is termed "Attenuation (Multiple Scatter)" in Figure 10. We assume the existence of at least dual scattering as sketched in Figure 9(c). Here the direct transmitter-receiver path establishes one signal phase and the path through S_1 and S_2 the second one. If this propagation mode is a valid one, inspection of Eq. (9) shows the appropriate expression

$$\frac{d\ell_1}{d\theta} = \frac{\ell\, d \sin\theta}{(\ell^2 + d^2 - 2\ell d \cos\theta)^{1/2}} . \qquad (12)$$

Eq. (12) can account for rapid phasing in an attenuation measurement, actually at half the rate observed for backscatter. This is apparent from an inspection of Figure 10.

A last interference mechanism affecting the attenuation measurement is possible by diffraction. At low grazing angles θ, radiation diffracted by the edge of the basket toward the receiver may be of comparable strength to the radiation transmitted directly through the snow slab. This is especially possible if the direct signal has been heavily attenuated by the snow. In terms of the rate range change, this mechanism is equal to single scatter as described in Eq. (9). The only difference lies in the distance d from the center of rotation. If d = 0.38 m is used for the edge of the basket rather than d = 0.12 m for the edge of the 3-dB beam, a curve in Figure 10 results quite similar to that labeled "Reflection". There is a substantial increase in the rate of range change over that for "Attenuation (Single Scatter)". This more rapid phasing should be noticeable only when the basket edge rotates enough to approach the edge of the transmit beam. Experimental results in Section 4 will be compared against those shown in Figure 10.

The change in received power as a function of grazing angle is another parameter aiding in the interpretation of millimeter-wave/snow interaction. Clapp,[13] in an early report on terrain reflection as seen by airborne radar, discusses three simple models: (a) diffuse reflection by the rough surface of a lossless medium, (b) omnidirectional direct reflection from a single layer of spherical particles with random mutual spacing, located approximately at equal height above a plane reflecting surface, and (c) omnidirectional reflection from the spherical particles of multiple stacked layers as in (b), such that multiple scattering occurs. The depth of layers is large enough to render background contributions to the backscattered signal insignificant. The absorption factor $(1 - \delta)$ as well as the spatial arrangement of spheres and the grazing angle relative to the "surface" of the medium determine the relative importance of first and higher order reflections.

Models (a) and (c) have the potential to represent granular snow quite well. Clapp assumes in (a) an angular distribution of scattered power according to Lambert's law. For unidirectional illumination as in the radar case, this can be achieved by a dissipationless dielectric. Due to multiple reflections and refractions, its reradiation characteristic is independent of the direction of the incident

13. Clapp, R. E. (1946) A Theoretical and Experimental Study of Radar Ground Return, Rep. 1024 Rad. Lab. MIT, Cambridge, Massachusetts.

radiation. Reradiated power density changes with the sine of grazing angle θ. Since the incident power per unit surface area is also proportional to $\sin\theta$, backscatter from a rough surface obeying Lambert's law is proportional to $\sin^2\theta$.

Model (c) is based on the assumption of a mean free pathlength between spheres much smaller than the thickness of the medium. This is the case for typical snow slabs. Another assumption is that of uniform reradiation from the spheres. This may or may not be true for granular ice particles at millimeter wavelengths. For lack of a better model it will have to be accepted here. If the spheres are lossy ($\delta \to 0$), single reflections predominate, leading to an angular dependence of reflected power proportional to $\sin\theta$. With $\delta \to 1$, second, third, and higher order reflections contribute significantly to the backscattered power. The θ-dependence becomes more complex. Equations based on up to third order reflections are included in Clapp's report. For the purpose of comparison with our experimental data we have replotted in Figure 11 his model (a) rough surface scatter and model (c) volume scatter including third order reflections, both for a lossless medium. In addition, the specular reflection model for backscatter is shown in the same figure. It is simply determined by the product of transmit and receive beam patterns. Since actual 3-dB beamwidths range from 6.8 to 13.9 deg, the curve in Figure 11 is for an average 9 deg. All three curves have been normalized to 0 dB at perpendicular incidence (θ = 90 deg). The curve labeled "Rough Surface Scatter" follows $\sin^2\theta$ exactly, while the curve labeled "Volume Scatter" drops off more strongly with decreasing θ than $\sin\theta$ would. This is the effect of multiple scattering. Note that the increase in scattered signal intensity in the perpendicular direction (θ = 90 deg) due to multiple reflections has been eliminated in the normalization process.

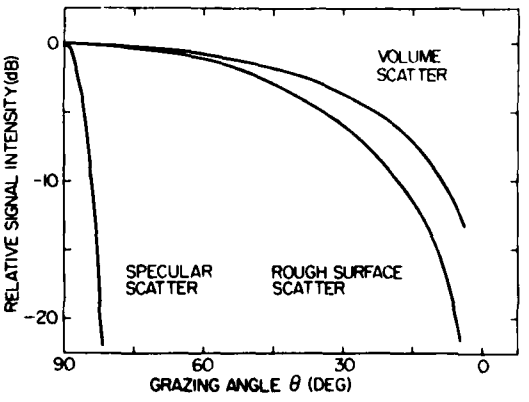

Figure 11. Angular Dependence of Backscattered Power

2.4 Measurement Procedures and Locations

One area of concern in the calibration of the sample measurements is the return from the waxed string or nylon fishing line holding the snow, and from the wooden frame of the sample holder. A series of measurements were made with the sample holder empty but fully strung with crosswoven 5 × 5-cm netting, and also with the sample holder empty and some or all of the strings removed. The majority of data in this report were obtained with all strings mounted along the direction perpendicular to the basket axis of rotation and two each at the end of the basket crosswise for better support of the slab (Figure 1). Measurements on the empty holder were made for horizontal, vertical, or crossed polarization at the three frequencies. Returns from the netting relative to that from the horizontally or vertically polarized return from the metal plate are listed in Table 2.

Table 2. Backscatter From Sample Holder

Polarization	Frequency (GHz) 35	98	140
HH	-50 dB	-30 dB	-38 dB
VV	-50 dB	-26 dB	-29 dB
HV	-50 dB	-50 dB	-48 dB

Here, H stands for horizontal and V stands for vertical polarization, with the first letter denoting the transmitted and the second letter denoting the received polarization. In none of the snow slab measurements was the return less than -20 dB. The contribution of the netting is therefore considered insignificant.

Snow measurements during the winter of 1977/78 were closely linked to the evolution of the equipment from the sample configuration to the in-situ configuration.[14] Measurements during the early part of the winter were conducted at the Prospect Hill Field Station at an elevation of 145 m above sea level. The equipment was positioned on a loading platform with a major part of it inside a heated building and only the boom extending outside. A plastic window closed the opening and prevented a temperature change around the snow slab due to heat generated inside the building. The loading platform afforded an additional 1-m separation of the test path from the ground, further reducing the possibility of unwanted reflection.

14. Hayes, D.T., Lammers, U.H.W., and Marr, R.A. (1981) Scattering From Snow Background at 35, 98, and 140 GHz, RADC-TR (to be published).

Snow slabs of proper size were cut from undisturbed areas in the vicinity. In most cases slabs were placed in the sample holder and left there until completion of the measurements. A complete set of measurements on a particular sample consisted of HH, VV, and HV scans at all frequencies, including a calibration against the metal plate before and after each scan. Sample measurements were begun 16 January 1978 and concluded 2 March 1978. During this time, data from a total of 230 runs were collected.

3. SNOW CHARACTERIZATION

Snow deposited on the ground undergoes substantial changes while aging under various weather conditions. Changes in the physical properties of snow cover have a profound effect on its interaction with millimeter waves. An effort was therefore made during the experimental program to determine in detail the relevant physical properties of snow at or near the location where samples were removed.

3.1 Snow Development

In one aspect, the winter of 1977/78 was typical for the Boston area. The major snowstorms took place during the months of January and February. The winter was atypical in the cumulative amount of snow deposited and the large amounts delivered by several storms. A total of 215 cm of snow fell in the Boston area. This was more than double the average snowfall (100 cm) expected in a single season. On two occasions, record snowstorms occurred. The storm of 20 January deposited 56 cm of snow. This was a record for a 24-hr period. On 6 February the "biggest snowstorm ever" began. By the time this storm ended on 7 February, 76 cm of snow had been deposited. High winds associated with the storm, coming at the time of full moon, resulted in severe coastal flooding and destruction. At the conclusion of this storm an accumulated total of 180 cm had been deposited since the first snowstorm on 26 November 1977. Deep snow in the area generally does not last for a long time. Boston's location on the New England coast ensures a variability of weather (cold to warm, snow to rain) to prevent any buildup of snow over a full season. When measured a week after the 6 February storm, the snow depth at the Prospect Hill Field Station was 86 cm. Of this, 61 cm came from the last storm. The remainder had been deposited during two previous storms.

Whether the Boston area is to be hit by snow, rain, or a mixture of the two depends upon the track of the low pressure area which approaches from the south. If the low tracks to the west of the city, rain is brought on southwesterly winds. If there is a large mass of cold air hanging over Boston as the low approaches from

from the south, the precipitation begins as snow. As the warmer air circulating around the low displaces this colder air, the precipitation changes to sleet or freezing rain and eventually goes over to rain. On the other hand, if the low passes to the east of the city, precipitation in the form of snow is the result. In November, the most probable track of a storm is to the west of Boston. As the winter progresses, the most probable path moves eastward. In January, it lies to the east of Boston. Thus, November and December storms are more likely to produce rain or start off as snow and end as rain. January and February storms are most likely to bring only snow. Precipitation in the form of rain is not an improbable event, even in the later winter months. However, there is usually enough snow on the ground at this time so that not all is washed away if rain does occur.

It should be clear from the above discussion that winter weather in the Boston area is most variable and that precipitation in the form of rain is a possibility throughout the winter. Thus, partial melting and subsequent refreezing due to temperature changes from day to night and drenching by rain play an important role in modifying the structure of the snow already deposited on the ground.

Newly fallen snow in crystalline form will begin to undergo changes almost immediately. If the vertical temperature gradient through the snowpack is small, water molecules tend to sublime from the sharper edges of the snow crystal where the vapor pressure is high and condense in sections of the crystal where the radius of curvature is low (low vapor pressure).[15] This breaks up the crystalline structure of the snow. The snow crystals slowly metamorphose into small round ice grains. The ice grains continue to undergo changes. Vapor sublimes from the smaller ones and condenses on the larger ones. This entire process is called equitemperature metamorphism (ET). The rapidity of the change is proportional to the temperature of the snowpack. It is most rapid near 0°C and almost ceases at -40°C. When equilibrium is reached, the medium consists of grains of nearly identical size, and the density of the snow is roughly 0.6 g/cm^3.

If a strong temperature gradient exists in the snow, the water vapor tends to migrate from the warmer region (near the ground) toward the colder region, where it condenses. This is temperature gradient (TG) metamorphism. It is rarely seen in New England.

The dominant metamorphic process affecting snow in the Boston area is the so-called melt-freeze (MF) metamorphism. Typically, following a midwinter storm, high pressure settles over the area bringing in cold air. During this time, ET metamorphism is dominant. Eventually the high passes over the region, bringing southerly winds. The air temperature rises above freezing during the day or at

15. Perla, R. I., and Martinelli, M., Jr. (1976) Avalanche Handbook, Agriculture Handbook 489, U.S. Dept. of Agr., Forest Service.

least high enough that solar radiation causes appreciable melting to take place in the upper layer of the snow. The high may be followed by a low bringing in rain. In any case, free water appears in the upper snow layer. It filters down through the snow, forms a liquid layer around a snow grain, and possibly connects two grains by a liquid meniscus. At night the water refreezes. As a net result the ice grains grow in size (up to 2 or 3 mm) and the bearing strength of the snow layer increases. This process can take place most rapidly. Late in the season, just one warm day with strong solar heating followed by a cold night is enough to destroy all vestiges of the virgin snow and produce a hard layer of ice grains.

3.2 Snow Measurement

To provide the necessary supporting data for analysis of the electromagnetic scattering and attenuation, selected characteristics of the snow cover were recorded concurrently with the electromagnetic measurements. In addition, the development of the snow cover during the winter snow season was recorded in a daily weather diary. The following snow properties were measured on a daily basis:

(1) Depth,
(2) Density,
(3) Hardness,
(4) Temperature,
(5) Stratigraphy,
(6) Microstructure,
(7) Surface characteristics.

The majority of these properties were determined using equipment supplied in the U.S. Army Cold Regions Research and Engineering Laboratory (CRREL) snow observation kit, manufactured by Geotest Instrument Corporation, Wheeling, Illinois. With the exception of temperature, all properties were assumed to remain unchanged during a daily test period. The snow was characterized each day before the electromagnetic measurements were begun. The snow properties were recorded, and a surface sample (4 to 14 cm thick) was cut to be used in the scatterometer. A trench running into an area of unperturbed snow was established. Each day the trench was extended exposing virgin snow.

The following measurement techniques pertain to individual snow parameters:

(1) Snow Depth
The total snow depth in the trench was recorded daily.

(2) Snow Density
Snow-sampling tubes provided in the observation kit were 6 cm in diameter. Their volume was 500 cm^3. At least three horizontal samples were obtained daily from each snow layer.

(3) Hardness

The surface hardness was measured using a Canadian hardness gauge supplied with the CRREL kit. This gauge consists of a push-type spring balance with provision for mounting disks of various sizes on the end of the push rod. In operation, the disk is pressed against the snow surface and the reading on the push rod scale is noted when the surface ruptures. The gauge is calibrated in g/cm^2.

(4) Temperature

Bimetallic thermometers (range -50 to 20°C), supplied in the CRREL kit, were used to obtain a temperature profile of the snow cover. At least one reading per layer was made. For layers thicker than 10 cm, the snow temperature was measured at about 5-cm intervals. The air temperature was recorded at the same time.

(5) Stratigraphy

The thickness of all snow layers was measured. The presence of any ice layers and their thickness were noted.

(6) Microstructure

A sample of snow in each layer was examined to determine grain shape and size distribution. Photomacrographs of the snow grains were made with a millimeter grid in the background in order to record the grain shape and size distribution.

(7) Surface Characteristics

The surface properties were described from visual observation. Also, photographs of the surface were made. Data on mean surface height variation and surface features were recorded. Types of surface features noted were: ice layer at surface, roughness caused by windblown snow, or snow melt-freeze cycle.

Snow data are presented in the appendix. Data are given for every day on which electromagnetic tests were conducted. Reference will be made to these data when discussing experimental results in Section 4.

4. EXPERIMENTAL RESULTS

No free water was detectable in any of the snow slabs used for measurement. The air temperature never rose above 0°C during tests. The tests were always carried out in the shade to eliminate the possibility of melting caused by direct solar radiation. Signal strength was recorded by pen and ink plot only, with received amplitude along the Y-axis and sample holder angular position along the X-axis. Typical sample data are shown in Figures 12 through 15.

4.1 Sample Cases of Scatter and Attenuation

It is possible to divide the sample data period into two distinctive sections. The first group of data was collected from 16 January through 6 February. During this period the weather was quite variable. A number of snowstorms occurred with varying amounts of snowfall. Each storm ended with sleet or freezing rain, or the snowstorm was followed a few days later by periods of moderate to heavy rain. A total of 41 backscatter measurements were performed during this period including frequencies 35, 98, and 140 GHz and polarizations VV and HV. There were 26 attenuation measurements at the three frequencies and at VV polarization. No bistatic scatter measurements were made.

Due to the heavy blizzard on 6/7 February, non-essential travel was restricted statewide. Snowclogged roads leading to the test site were not cleared until 21 February, on which day measurements were resumed. The second period of sample measurements included 21 February to 2 March. The weather following the blizzard was marked by its uniformity. The days were sunny for the most part and the temperature rarely exceeded freezing. Only on three days did this occur: 2°C on 16 February, 3°C on 17 February, and 1°C on 24 February. The change in the deposited snow crystals proceeded by ET metamorphism at a very slow rate. By the time sample measurements were resumed on 21 February, the structure of the snow had reached a fairly stable equilibrium condition. During the course of measurements the properties of the snow essentially did not change. The variability of the samples collected on different days could be attributed to the horizontal inhomogeneities in the snow cover. These were caused by drifting and other factors such as variability in solar heat loading. Some samples were collected from areas which were continuously in the shade. A total of 71 backscatter and 53 bistatic scatter measurements were performed during this time. In both cases data were obtained at 35, 98, and 140 GHz and at HH, VV, and HV polarization. Attenuation measurements numbered 39 at the same frequencies and HH and VV polarization.

From the large set of data, three days were selected for discussion in this section. The specific days chosen display both distinctive physical characteristics of the snow and typical effects on the electromagnetic signals. Figures 12 and 13 represent unprocessed data from the earlier period. They are made up of six individual measurements each. Backscatter and attenuation at vertical polarization are shown for the three frequencies. The days chosen, 17 January and 28 January, are near the beginning and the end of the earlier period. They represent the variability of snow conditions and measured data during this time.

During this period two specific types of snow cover existed. On the first two days of testing, the top 5 cm of snow consisted almost entirely of spherical sleet particles. Data collected from a slab containing only the sleet layer are shown in

Figure 12. Subsequent snowstorms covered the sleet layer. Periods of rain followed which produced rapid change of the new top snow and the sleet layer. Examination of the layers showed typical effects of MF metamorphism. The sleet layer was perturbed by the rain to the point that it differed from the other layers only by a higher density. As the snow continued to age, the thickness of ice layers delineating the boundary between snow layers increased. The second set of backscatter and attenuation data (Figure 13) was collected using a 14-cm thick sample of this type of snow.

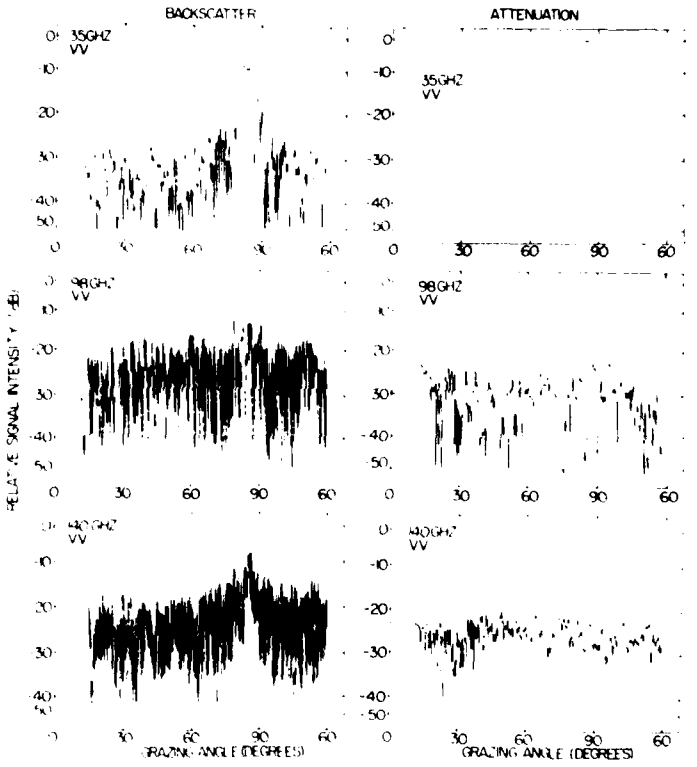

Figure 12. Sample Backscatter and Attenuation Data of 17 January 1978, (vertical polarization)

The third set is typical of data collected after the blizzard. At this time the measurement protocol had been expanded to include both horizontally polarized and bistatic measurements.

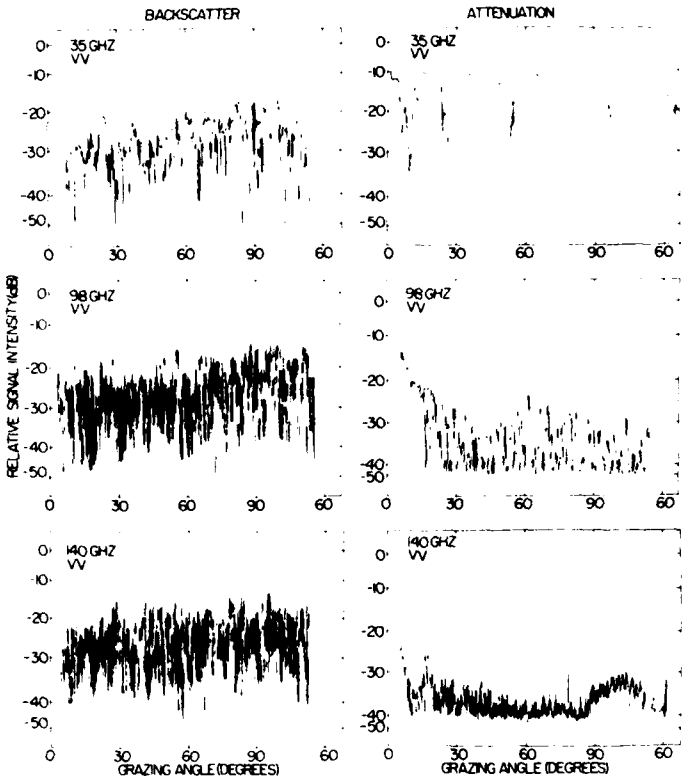

Figure 13. Sample Backscatter and Attenuation Data of 28 January 1978, (vertical polarization)

Figure 14 shows original co- and cross-polarized backscatter data collected at each frequency on 23 February. Figure 15 displays bistatic scatter and attenuation data collected on the same day. For approximately three weeks following the blizzard, the weather was sunny and cold, causing ET metamorphism. The average snow properties present in the periods from which these sample data were chosen are compiled in Table 3. The density (0.26 g/cm^3) of the samples collected following the blizzard did not differ much from that of the samples used in the latter part of the January tests (0.29 g/cm^3). However, there was a marked difference in the bearing strength of the snow cover between that produced by the MF metamorphism in January and that produced by ET metamorphism following the blizzard. The rains in January provided ample liquid water which upon freezing increased the strength of the bonds between adjacent snow grains. This resulted in a rigid material from which samples could be cut easily and removed without destroying the integrity of the sample.

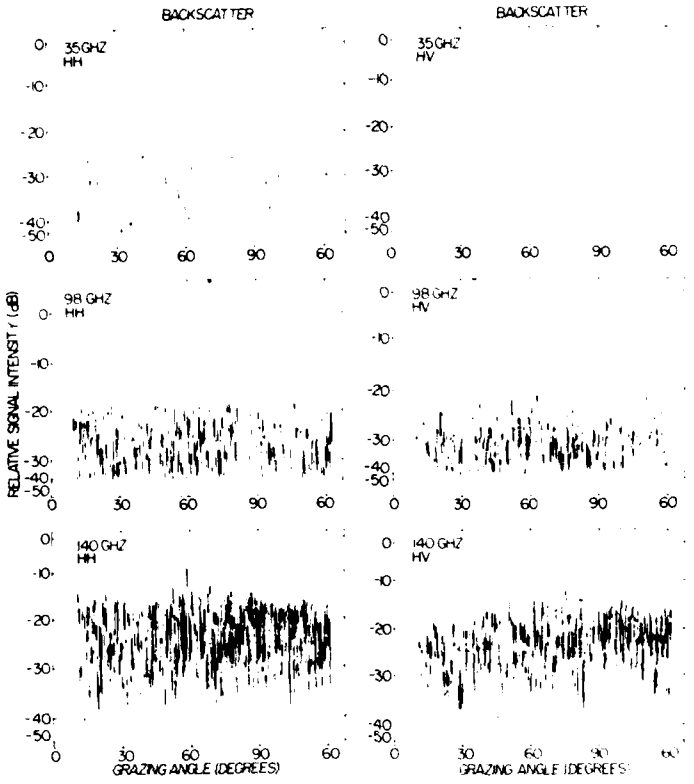

Figure 14. Sample Backscatter Data of 23 February 1978, (horizontal and cross-polarization)

During ET metamorphism, bonding between adjacent snow grains is produced primarily by sublimation. As a result, the bonds tend to be weak. This was the case with the snow after the blizzard. The top inch was a fairly rigid crust produced by solar melting during the day and refreezing at night. Below this the snow was fragile. Samples could be cut but great care had to be taken so as not to break the sample.

The data from each day will be considered in turn. The ordinate of each graph is labeled in dB below the signal received from the metal calibration plate. The compressed scale for lower signal levels is due to the receiver AGC characteristic. The abscissa is marked in degrees grazing angle of the transmitted beam on the snow surface. The grazing angle increases from 0 to 90 deg and then decreases to 60 deg, even though the graph represents a one-directional motion of the basket, covering an angle of 120 deg. This is done so that the grazing angle remains an acute angle between the transmitted beam and the snow surface. The backscatter

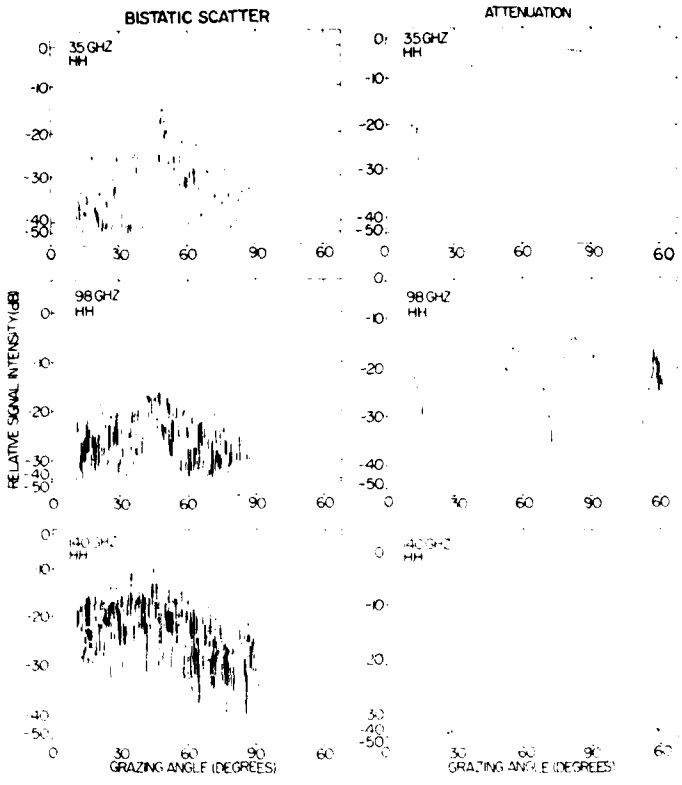

Figure 15. Sample Bistatic Scatter and Attenuation Data of 23 February 1978, (horizontal polarization)

return at 35 GHz from the sleet sample (Figure 12) is quite specular in nature. For comparison purposes the return at 35 GHz from the calibration plate is shown in Figure 16. The return from the sleet slab is about 10 dB below the peak signal from the flat plate. This is close to the reflected power one would calculate from a flat slab of ice. Using Stratton's[16] expression for the power reflection coefficient (perpendicular incidence on lossless dielectric)

$$R(dB) = 20 \log \frac{n_r - 1}{n_r + 1}, \qquad (13)$$

one obtains R = -11 dB for $n_r = 1.78$, the value for ice given by Ray.[11]

16. Stratton, J.A. (1941) Electromagnetic Theory, McGraw-Hill, New York.

Table 3. Average Parameters of Snow Cover

Time Period	Average Density (g/cm^3)	Average Grain Size (mm)	Grain Shape	Comments
16 January and 17 January	0.53	2	Spherical	Sleet (Firm structure)
27 January to 6 February	0.29	1 (Many bonded together to 2, some to 4 mm)	Irregular	Melt-Freeze Snow (Very firm structure)
21 February to 2 March	0.26	1	Irregular	Equitemp. Snow (Very brittle structure)

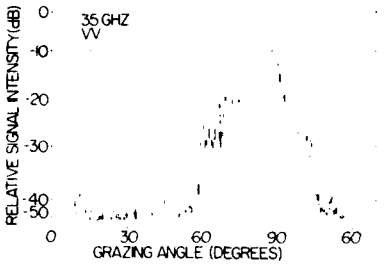

Figure 16. Backscatter From Flat Metal Plate at 35 GHz, (vertical polarization)

The backscattered signal at slab directions other than perpendicular exhibits the scintillations one expects from a random collection of scatterers, in this case the sleet particles.

At 98 and 140 GHz much less of a specular response is seen. The appearance of the fluctuating signal is essentially unchanged at all grazing angles. At both frequencies, the peak return at perpendicular incidence is again below that from the flat plate by approximately 10 dB. Thus it is roughly equal to the power reflected from an ice slab. As the grazing angle decreases, the backscatter signal decreases only slightly. It must be assumed that an effective backscatter mechanism exists within the invididual scattering particle. Incoherent contributions from many particles add up to a strong sum signal. Backscatter from dielectric spheres near resonance could account for this result.

The character of the attenuation data also differs between 35 GHz and the two higher frequencies. With the exception of grazing angles below 30 deg, no attenuation was measured at 35 GHz. The transmitted signal is independent of the angular

position of the basket. At the two higher frequencies the transmitted signals are strongly attenuated and modulated in a complex fashion. The modulation of the transmitted signal at angles larger than 30 deg appears to be composed of a slowly varying component of large amplitude with a more rapidly varying component of lower amplitude superimposed on it. Below 30 deg there is a change in the character of the modulation.

A number of changes can be seen in the data (Figure 13) collected from melt-freeze snow. First, there is no trace of a specular return at 35 GHz. Second, the backscattered signal at lower grazing angles is higher than the return measured from the sample containing sleet. Third, the 35-GHz signal is attenuated and modulated upon transmission through the snow. The differences in the nature of the 35-GHz data collected from the two samples allow the following conclusion. In the case of the slab containing sleet, the strong coherent specular reflection and the strong coherent transmitted signal completely dominate any incoherent scattering caused by individual snow grains. Only for backscatter at grazing angles such that the receiving antenna does not intercept the specularly scattered power does one see a fluctuating signal indicative of scattering from a collection of random scatterers.

In contrast, the sample of melt-freeze snow causes strong incoherent scattering. The coherent backward and forward propagating signals are decreased to the point that incoherently scattered power dominates and one sees a randomly modulated signal at all grazing angles. The backscatter signals at the higher frequencies are somewhat lower than those for the corresponding sleet data. Aside from this, the character of the backscatter signal is not changed. The transmitted signals are different. First, they are more strongly attenuated. This is to be expected as the slab is thicker (14 cm as opposed to the 5 cm sleet slab). Second, the modulation frequency of the transmitted signal is higher. At 140 GHz, the fluctuation frequency of the transmitted signal is comparable to that of the backscattered signal. This again may be due to the thicker slab giving more opportunity for multiple scattering. Also, individual ice particles in melt-freeze snow may be stronger scatterers. Visual examination of the snow showed clusters of ice grains forming macrograins, roughly spherical in shape with diameters as large as 1 cm. Herman and Battan[17] have calculated the backscatter cross section of ice spheres. They have shown that the backscatter cross section (normalized to the geometrical cross section) is an oscillatory function whose mean value increases as a function of $2\pi a/\lambda$ (a is the sphere radius). It reaches a maximum of 40 at $2\pi a/\lambda \approx 60$, before decreasing asymptotically to 0.078 as $2\pi a/\lambda$ approaches infinity. Increased snow grain size could produce greater backscatter and attenuation.

17. Herman, B. M., and Battan, L. J. (1961) Calculations of Mie backscattering of microwaves from ice spheres, Quart. J. of the Roy. Met. Soc. 87:223-230.

Finally, consider the unprocessed data collected on 23 February. A specular backscatter signal is seen at 35 GHz (left-hand side of Figure 14), but it appears weaker than that measured off the sleet sample on 17 January. The backscatter returns determined at 98 and 140 GHz are very similar to those from the sleet and melt-freeze snow samples. The cross-polarized backscatter signal is shown on the right-hand side of Figure 14. The 35-GHz cross-polarized return displays no specular response and is always more than 35 dB below the co-polarized metal-plate return. Compared to the co-polarized signal from the snow, the cross-polarized signal was about 20 dB below at perpendicular orientation and about 10 dB below at other angles. The situation is different at 98 and 140 GHz. At 98 GHz the cross-polarized return is never more than 4 dB below the co-polarized return. The co- and cross-polarized signals are somewhat comparable also at 140 GHz. At both frequencies the appearance of the fluctuating signals is similar.

The bistatic return is shown on the left-hand side of Figure 15. During the bistatic measurements, the difference between the transmit and the receive beam directions was set to 90 deg. All bistatic data were obtained at this single constant scatter angle. At each frequency the envelope of the fluctuating signal has a maximum at 45 deg grazing angle and falls off to either side of this angle. At 45 deg, we expect the maximum specularly reflected signal to occur. The drop-off is sharpest at 35 GHz. The specular appearance at this frequency is comparable to that in the backscatter mode. It is interesting to note that at 98 and 140 GHz the bistatic scatter signal shows an angular dependence distinctly more influenced by the specular mechanism than the backscatter signal. This can be qualitatively understood in the following way. The individual scatterers in the top layer of the snow, which is most active in scattering, have certain random excursions in height from the average surface plane. In terms of the Rayleigh criterion the sum signal from the individual sources will be more coherent the lower the frequency and the lower the scattering angle. This means, for a given snow surface and frequency, bistatic returns are more coherent as seen in Figures 14 and 15. In the extreme case of very low scattering angles this has been demonstrated by our multipath propagation measurements.[12]

Transmission measurements through this snow at 35 GHz produced a result intermediate to that measured through the slab of sleet and the slab of melt-freeze snow. The slab containing sleet caused almost no modulation of the transmitted signal, and the melt-freeze snow resulted in a transmitted signal modulated over the entire angular range. In the case of ET metamorphic snow there is a weak increase in the transmitted signal on both sides of perpendicular incidence. From a grazing angle of 45 deg on down, the transmitted signal level decreases while superimposed by a gentle modulation. Below 20 deg, the modulation changes to a series

of abrupt and deep fades. The increase in signal level at very low grazing angle due to diffraction around the edge of the basket does not show in this graph as it did in the other attenuation measurements at this and the higher frequencies. The 98- and 140-GHz plots also show notable differences with regard to the earlier figures. At 98 GHz, attenuation is generally lower than in the previous cases with the exception of a few deep nulls, one peculiarly located at around 70 deg grazing angle. The fluctuation rates compare somewhat with those seen for sleet and melt-freeze snow. This is in contrast with the 140-GHz data. They show higher attenuation than in Figure 12 with a similar number of fluctuations, but similar attenuation as in Figure 13 with a lower number of fluctuations. It is apparent from this discussion of sample cases that results are not always systematic or at least not easily explainable in terms of snow parameters observed.

The data collected after the blizzard constitute the largest number of cases with only limited changes in snow characteristics. They will be used here for comparisons of fluctuation rates and signal level change with grazing angle as previously developed from the models. Based on the appropriate curve of Figure 10, a value for the number of backscatter signal fluctuations per deg was calculated at 35, 98, and 140 GHz at grazing angles of 90, 45, and 15 deg. The results are plotted in Figure 17 as three dashed curves, each representing one of the three frequencies. In the same figure, the three solid curves represent the corresponding fluctuation rates derived from the measured data. The measured values were arrived at by counting the number of fluctuations occurring within 5 deg of either side of grazing angles of 90, 45, and 15 deg. Average rates were those derived from 20 data runs at 35 GHz, 16 runs at 98 GHz, and 14 runs at 140 GHz. One observation, when inspecting Figure 17, is a measured fluctuation rate greater than that predicted at all frequencies and at all grazing angles. This is particularly evident at the lower grazing angles where, for example, the ratio of measured and predicted rates approaches 4 at 140 GHz and 15 deg. The model used to derive backscatter fluctuation rates assumes single scattering. It also considers only the phase interference between a scatterer at a fixed distance d from the center of rotation and a scatterer immobile at the center of rotation. This would tend to represent the true case at perpendicular orientation of snow surface and transmitter beam. When the slab tilts relative to the beam for a lower grazing angle, the edge of the 3-dB beam corresponds to a larger d (the larger half-axis of the elliptical antenna footprint). At a grazing angle of 15 deg, d has increased by a factor of 2.7 in this direction. If we further consider that the radar range-factor puts the closest portion of the footprint at a noticeable advantage in terms of power received per unit scattering area, this could account for the discrepancy between calculated and measured fluctuation rates. A more elaborate model is in order for the backscatter case. Multiple scattering might be a contributing factor, but is not required to explain the experimental results. Averaging of the number of fluctuations within a 10-deg

interval is a subjective procedure. It must account for part of the differences observed.

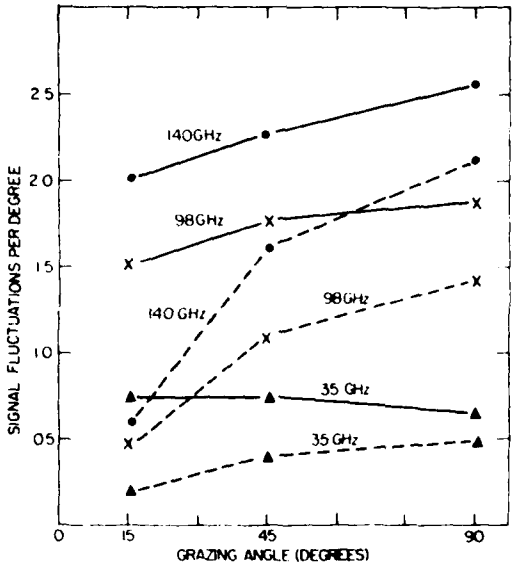

Figure 17. Measured (—) and Predicted (---) Backscatter Fluctuation Rates

Because of the more limited angular range, over which bistatic scatter data were observable, no attempt was made to verify the model fluctuation rates in Figure 10. It is clear in the bistatic case that the elliptical shape of the scattering area on snow also leads to higher fluctuation rates at low grazing angles than calculated for a circular area.

It has been demonstrated by the sample cases that upon transmission through snow, the received signal level varies in a complex manner with changing direction of penetration. We had modeled four different mechanisms in Figure 10 which could explain interaction of multiple signals in the transmission mode. At low grazing angles, a signal diffracted around the outer edge of the basket compares well with that transmitted at an oblique angle through the snow. The oblique path through the snow is longer than the thickness of the slab. It depends on the type of snow, thickness, and frequency at which basket angle the diffracted signal becomes a significant portion of the total signal received. Diffraction effects must be seen as an undesired side effect of our measurement setup. For each plot of the post-blizzard data, a grazing angle was established below which the fluctuations were attributed to diffraction. The number of fluctuations was counted. Average numbers

for all attenuation plots from this period are listed in Table 4. Measured numbers of fluctuations are those between 10 deg and the average angle of onset. Note that this latter angle increases with frequency as can be expected. Predicted numbers are based on an average rate of range change of 1.9 mm/deg, estimated from Figure 10 in the diffraction region. Remember that the curve labeled "Reflection" approximates the one for diffraction. Specific numbers in Table 4 represent 1.9 times the deg-range of diffraction, divided by wavelength. The results support the assumption of diffracted signals.

Table 4. Fluctuation Characteristics of Attenuated Signal

Frequency (GHz)		35	98	140
Diffraction Region	Average Angle of Onset (deg)	22.2	27.3	29.4
	Measured Number of Fluctuations	3.1	13.3	18.4
	Predicted Number of Fluctuations	2.7	11.0	18.5
30- to 90- to 60-deg Region	Measured Number of Slow Fluctuations	——	15.9	24.0
	Predicted Number of Slow Fluctuations	2.7	7.8	11.8
30- to 90- to 60-deg Region	Measured Number of Fast Fluctuations	——	54.0	84.2
	Predicted Number of Fast Fluctuations	20.9	60.0	90.0

The other three mechanisms, suggested for the explanation of observed fluctuations, are single and multiple scattering and reflection off the snow/air interfaces. If one mechanism were predominant, measurements should identify it by its characteristic angular dependence. Unfortunately, results do not bear this out very well. If signals due to scattering and reflection reach comparable amplitudes, the angular variation becomes inconclusive. In Table 4 we have therefore shown total numbers of fluctuations over the 90-deg interval of basket rotation outside the diffraction region. Measured data are again averages over all available plots. As it generally appeared that fluctuations could be grouped into fast and slow ones, these have been counted separately. It is not clear that single and multiple scattering should lead to such a distinctive distribution of fluctuation rates. For the sake of a simple comparison, we have assumed that "Single Scatter" in the 30- to 90- to 60-deg

region predicts an upper bound of 0.25 mm/deg for the rate of range change. The corresponding number of "Multiple Scatter" is 2.1 mm/deg. Multiplying these numbers by the deg-range of observation and dividing by wavelength yields the predicted numbers of slow and fast fluctuations, respectively.

Table 4 omits measured data in the 30- to 90- to 60-deg region at 35 GHz. Fluctuations were non-existing or too inconsistent to arrive at meaningful values at this frequency. At 98 GHz and 140 GHz the number of observed fast fluctuations is indeed bounded by the prediction. However, observed numbers of slow fluctuations are higher by a factor of 2 or more than predicted. No further conclusions will be drawn from this, since the model apparently does not match the complexity of the real situation.

4.2 Summary of Experimental Data

While discussing the results of all scatter and attenuation measurements obtained on snow samples, reference will be made to meteorological observations and measurements of physical snow parameters or ground truth data as they are called in reference to millimeter-wave imaging systems. These data are compiled into tables. In the appendix, one table is given for each of the 20 days, on which scatter and attenuation measurements were made. The data underline the structural and developmental variability of a medium which is not obvious to the casual observer. The surface of snow cover may also vary substantially in terms of the wavelengths of interest here. For illustration purposes, two of the slabs used in the experiments are shown in Figures 18 and 19. The surface of a slab cut on 2 March from ET snow is almost smooth (Figure 18). In contrast, Figure 19 displays a slab with a heavily cusped surface. It was cut on 2 February and owes its surface structure to MF metamorphism.

All data presented in this section are average peak values. Referring back to the original data plots in Figures 12 through 15, the only practical way to manually derive average signal levels from these plots was to average the local peaks of the rapidly fluctuating signals. An analysis of how these average peak signals relate to mean signal levels will be included in the forthcoming report on in-situ snow scatter measurements.[14] Bear in mind that all subsequent graphs in this report pertaining to actually measured data represent averages of peaks.

Based on the mode of operation of the equipment (continuous measurements are made while the basket rotates), data exist for a contiguous range of grazing angles θ. In the in-situ configuration, grazing angles had to be chosen parametrically to limit the total number of measurements. Values for θ selected were 90, 45, and 15 deg. The lowest angle over terrain is dictated both by system sensitivity and the physical limits of the snow field.

For reasons of comparison between the two modes of operation as well as simplified data processing, sample data were processed and plotted at the same three grazing angles.

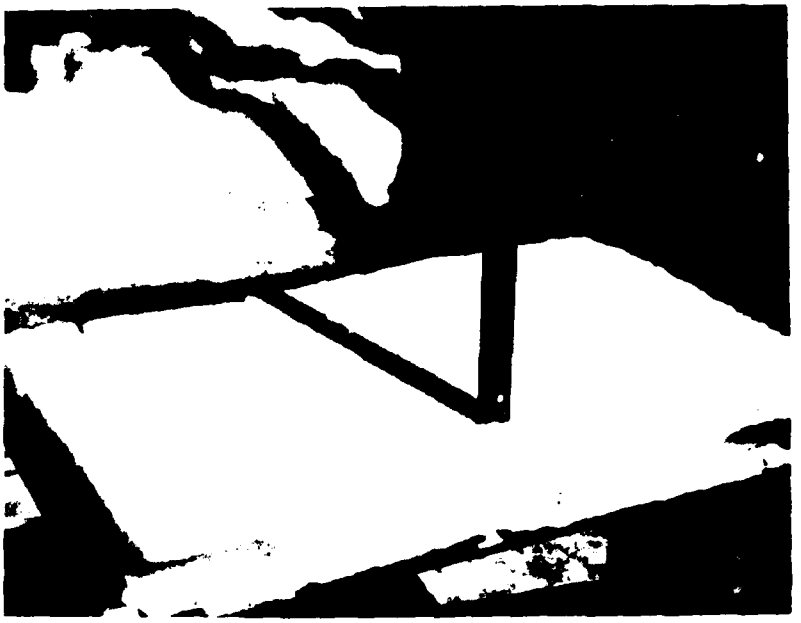

Figure 18. Typical Smooth Sample of Equitemperature Snow, (edges were intact during tests)

4.2.1 BACKSCATTER DATA

Consider first the slab data collected in the period of variable weather conditions (16 January to 2 February). Figure 20 shows the backscatter coefficient σ° vs grazing angle measured on 16 January. Each frequency (35, 98, and 140 GHz) is represented by an individual curve. The sample used to gather these data was made up of the top hard layer of the snow cover, 4 cm thick. This layer consisted entirely of sleet deposited at the end of the snowstorm of 14 January. The almost perfectly spherical sleet particles varied in diameter from 1 to 3 mm, the prevalent size being 2 mm. When the sleet particles fell, they were covered by a thin layer of water. Upon deposit and subsequent temperature drop below freezing, the particles became firmly attached to each other, thus forming a very hard structure. The surface easily supported the weight of an adult walking across it. With the

exception of a 1-mm thick layer of ice at the surface, the sleet particles retained their spherical shape in the fused state.

Figure 19. Typical Sample of Melt-Freeze Snow With Cusped Surface

Examining Figure 20 at a grazing angle of 90 deg, one sees that the backscatter coefficients σ^0 are essentially equal (10 to 11.5 dB) at all frequencies. At 98 GHz, σ^0 decreases to -9 dB at 45 deg, and to -14 dB at 1 deg. For 140 GHz from the value at 90 deg exceeding 20 dB. The decrease in σ^0 with decreasing angle is less pronounced at the two higher frequencies. At 98 and 140 GHz the dependence is almost a linear function of the grazing angle when σ^0 is expressed in dB. At a grazing angle of 1 deg, σ^0 equals -6 dB at 98 GHz and -3 dB at 140 GHz. For angles other than 90 deg, the value of σ^0 increases as a function of frequency. This relationship holds true for all data in the report.

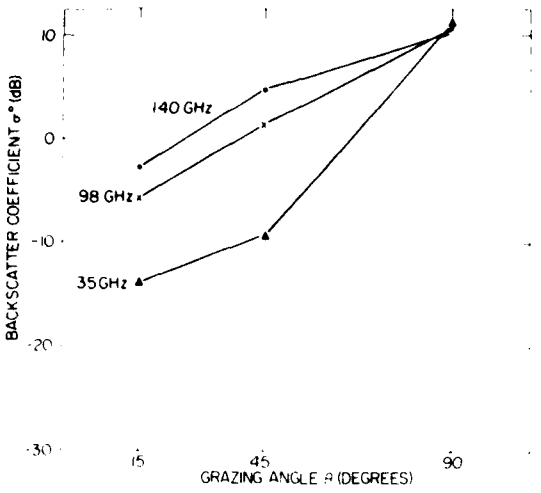

Figure 20. Backscatter Coefficient From Sleet, (data of 16 January 1978, vertical polarization)

On 17 January, the condition of the snow was essentially unchanged from that of the previous day. The backscatter experiment was repeated, again at vertical polarization. Measurements of σ° at 45 and 15 deg were almost unchanged. At 90 deg, there was a 5-dB spread. At 35 GHz, σ° was found to be 11 dB, hardly changed from the previous day. At 98 GHz, a decrease by 3 dB to 8 dB was observed. At 140 GHz the change was positive by 2.5 dB to 13.5 dB.

On 18 January, a heavy rain/snow storm took place which deposited 5 to 8 cm of wet, irregularly shaped ice grains on top of the existing snow cover. The mean diameter of the grains was approximately 1 mm. Following this, a severe snowstorm hit on 20 January. A record snow accumulation for a 24-hr period of 56 cm was measured in Boston. No rain was associated with this storm which was followed by clear, cold (subfreezing) days. The next set of backscatter measurements were performed on 24 January. The backscatter coefficients measured on this day are shown in Figure 21. The snow parameters of the slab used are given in the appendix. The sample had been cut for use on 19 January. However, it was not used as tests were stopped in order to modify the basket drive mechanism. Until testing resumed on 21 January, the slab lay horizontally on a platform at the test site. During this time, snow from the 20 January storm was deposited on the slab. A top layer formed, 3.5-cm thick, with a density of approximately 0.25 g/cm^3. Under the new snow, a 3-cm layer of irregularly shaped ice grains of 1 to 2 mm diameter had a density of 0.38 g/cm^3. This layer had been deposited in the rain/snow storm of 18 January. Under this lay a 4.5-cm thick layer of the dense (0.53 g/cm^3) snow, used in the tests of 16 and 17 January.

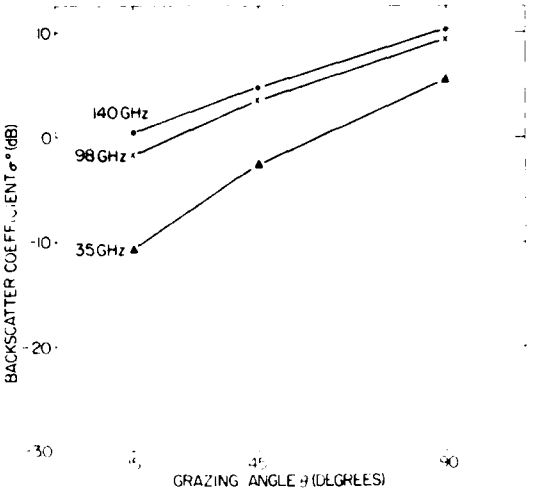

Figure 21. Backscatter Coefficient From Melt-Freeze Snow, (data of 24 January 1978, vertical polarization)

There is a marked change in the angular dependence of the backscatter coefficient especially at 35 GHz. At this frequency, at a grazing angle of 90 deg, σ° has dropped by 5 dB relative to the level of 16 January. At the shallower angles of 45 and 15 deg, the backscatter coefficient has increased by 6 and 3 dB, respectively. The newer, less dense top snow had removed all indications of a specular nature of the backscatter coefficient. There is a lesser change in σ° at 98 and 140 GHz. At 90 deg, the value of σ° is essentially unchanged. At 45 and 15 deg, the 98-GHz value has increased by approximately 3 dB. At 140 GHz, σ° has increased by 3 dB at 15 deg but is unchanged at 45 deg.

Rain fell on 25 and 26 January, followed by sunny and cold days up to 6 February when the tests were stopped due to heavy snowfall. Additional backscatter measurements were made on 27, 28, 30, 31 January and 1, 2, 4, 6 February. The sample slabs were cut from the upper 10 cm of snow cover and, with the exception of a lower ice layer, consisted entirely of snow deposited in the storm of 20 January. To determine the effect of the ice layer, some of the tests were repeated following removal of the ice layer. No change in σ° was detected.

According to the tables in the appendix, the volume characteristics (density, temperature, and so on) of the snow did not vary much during this period. The rainstorms of 25 and 26 January did cause cusp-shaped depressions to be formed on the snow surface. An example of this phenomenon was shown in Figure 19. The cusps were about 1 cm deep and about 5 cm in diameter. Some 11 cusps were counted per meter. Nonetheless, the snow return did not change appreciably during this period. This is illustrated in Figure 22. The average of the data collected on 16 and 17 January is shown as solid lines. The dashed lines are the result of

averaging all data collected in the period from 24 January to 6 February. Comparing the dashed curves in Figure 22 with the data of 24 January in Figure 21, one sees only small changes at each grazing angle and frequency. In contrast, the differences between the solid and dashed curves in Figure 22 are more significant.

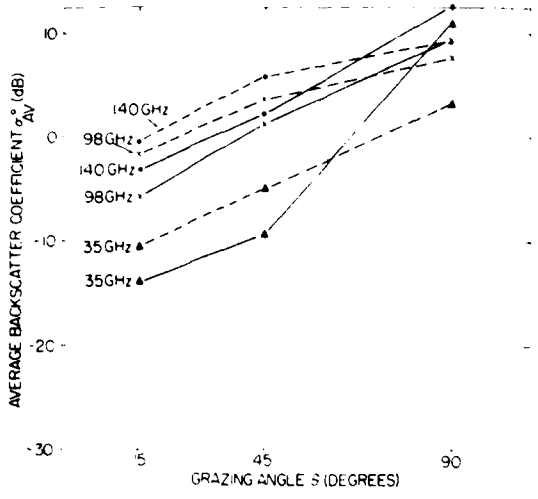

Figure 22. Average Backscatter Coefficient From Sleet, (—data of 16 and 17 January 1978) and From Melt-Freeze Snow, (--- data of 24 January to 6 February 1978), Vertical Polarization

The test program was expanded following the blizzard of 6 February. In addition to collecting data at vertical polarization, measurements were made at horizontal polarization and in the cross-polarized mode. During the two-week period from the end of the storm to the resumption of the measurements on 21 February, metamorphism proceeded primarily by the ET route. This is a slow process compared to that brought about by the heavy rain/snow storms in January. However, it appears that two weeks were sufficient for the process to reach an equilibrium state.

With the exception of a test to be discussed later, all tests conducted in this period used snow samples which were 12.7 cm thick. Reference to the ground truth data (see Appendix A) shows that the top 2.5 cm of each sample consisted of a layer of crust. This layer was produced by solar heating and melting of the snow during the day and subsequent refreezing at night. The remaining snow below this layer was composed of grains produced by ET metamorphism. The grains were only weakly bound together, producing a fragile sample which was supported mostly by the crustal layer. The density in these samples (0.26 g/cm^3) was roughly the same as in the samples used in January. The grain sizes were also similar.

Data were gathered on 7 days in the period from 21 February through 2 March. Each day the sequence of scatter and transmission measurements at polarizations VV, HH, and HV started with a different frequency. The sequence was then repeated at the other two frequencies. A single snow sample was used for each day's tests. Following the completion of the measurements, a run duplicating the initial one of the day was made. The purpose was to establish that no major change in the sample properties had occurred during the test period. A different frequency was chosen on a rotational basis to begin the tests on different days.

Since the properties of the samples did not vary much from day to day, data gathered on individual days will not be considered separately. Instead, like data from each day have been averaged together. The average backscatter coefficient as a function of the grazing angle is presented in Figure 23 for each frequency and polarization. Compare the backscatter coefficient for vertical polarization (dashed lines in Figure 23) with the corresponding data in the January tests (dashed lines in Figure 22). The 35-GHz data in each figure show the backscatter coefficients at 90 deg as equal. At 45 and 15 deg, average backscatter returns measured from the February snow samples at 35 GHz are 3 to 4 dB below those measured from the January samples. At 98 GHz, the average return from the February snow is approximately 3 dB lower at each grazing angle. The return at 140 GHz off February samples is 1 to 2 dB higher than that measured in January.

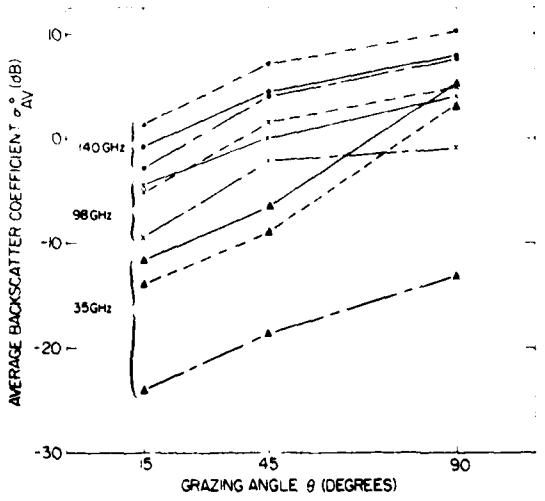

Figure 23. Average Backscatter Coefficient From Equitemperature Snow, (data of 21 February to 2 March 1978, polarizations HH —, VV ---, HV - - - -)

The average 35-GHz backscatter coefficient at horizontal polarization exceeds the corresponding values at vertical polarization by about 2 dB. At 98 GHz, the

values of these quantities are roughly equal. The average values of the backscatter coefficient for horizontal polarization at 140 GHz is approximately 2 dB less than that for vertical polarization at all grazing angles. The cross-polarized backscatter coefficient σ°_{HV} displays an interesting behavior. At 35 GHz, σ°_{HV} is 18 dB lower than σ°_{HH} at a grazing angle of 90 deg and 12 dB lower at 45 and 15 deg. The angular dependence of σ°_{HH} and σ°_{VV} at 35 GHz is somewhat specular (similar to the early sleet samples), and the small levels of the cross-polarized component relative to the like-polarized levels are further indication of scattering from a surface which appears smooth at the particular wavelength (35 GHz). A dramatic change in σ°_{HV} is seen as the frequency is increased. The strength of the cross-polarized return relative to the like-polarized return goes up with frequency. At 98 GHz, the cross-polarized σ° is, on the average, only 5 dB below the like-polarized σ°. At the highest frequency, 140 GHz, the average cross-polarized and horizontal like-polarized backscatter coefficients are almost equal.

As has already been mentioned, the snow samples used in the February tests were covered by a 2- to 3-cm thick crust. To determine the strength of the backscatter from the crust relative to that from the full slab, measurements were made in one case on the crust alone. The sample was cut to conform to the standard thickness for this series (12.7 cm) and the backscatter coefficient determined at 98 GHz. Following this run, the bottom 10-cm of fragile snow was removed from the sample, leaving only the crust in place. Then, the backscatter measurement was repeated using the thinner sample. After this, the thin sample was used to measure the backscatter coefficients at 35 and 140 GHz. The results at 98 GHz using the original 12.7-cm sample agreed to within 1 dB with those measured on the thin (2.5 cm) sample. Since 98 GHz was the only frequency at which a direct comparison was possible, at the other two frequencies a comparison was made against averages of samples consisting of crust and underlying fragile snow from the whole period. To illustrate the general trend, values of σ°_{VV} and σ°_{HH} obtained from the crust only have been averaged together. In Figure 24, these values connected by dashed lines are plotted for [illegible] as a function of the grazing angle. The averages of σ°_{VV} and σ°_{HH} [illegible] from the thicker samples are shown in Figure 24 by solid lines. [illegible] thin-crust comparison against the average of the thick-sample [illegible] agreement like that against the single thick sample. This suggests that [illegible] scattering is not taking place at depths beyond 2.5 cm. Attenuation coefficients in the next section support the assumption. At 35 GHz, deeper penetration into the slab must be expected, and the higher backscatter coefficients shown in Figure 24 are plausible. There is no simple explanation as to why the 140-GHz results should show the same trend. This is particularly so, since the 98-GHz results indicate that the effect of the fragile

snow was small. It must be kept in mind that this was only a single case of thin snow crust.

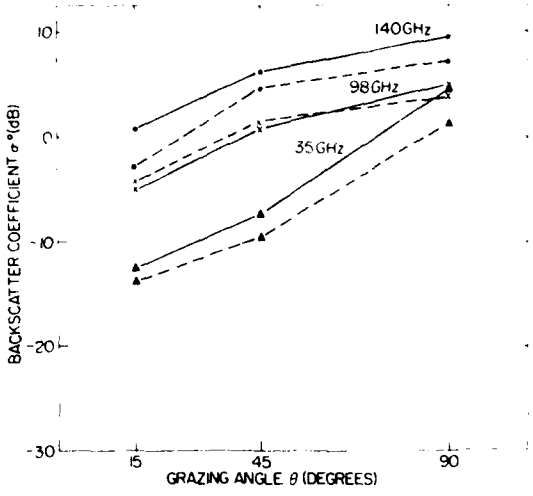

Figure 24. Comparison of Backscatter Coefficient Measured off Thick and Thin Snow Slabs, (12.7-cm slab —, 2.5-cm slab - - -)

The angular dependence of scattered signal intensity as a function of grazing angle according to Clapp's models[13] could shed additional light on the scattering mechanisms of metamorphic snow. A volume-scattering medium would be distinguishable by an angular σ°-dependence following a $\sin\theta$-law. A surface-scattering medium would display a $\sin^2\theta$-dependence on grazing angle. Specular reflection would be indicated by an angular dependence proportional to the product of the antenna patterns. Referring back to Figure 11, a volume-scattering medium fitting Clapp's model exhibits a decrease in scattered power of 1.8 dB between grazing angles of 90 and 45 deg. At 15 deg, the scattered power has dropped to 7.3 dB below that for perpendicular incidence. Rough-surface scattering according to Clapp's model is indicated by a signal drop-off of 2.9 and 11.5 dB at the lower grazing angles. True specular scattering measured with the average beamwidth used in the scatterometers requires a signal reduction by 10 dB within 6 deg from perpendicular incidence.

Theoretical curves were plotted and overlaid onto the average backscatter curves for sleet and MF snow in Figure 22 and for ET snow in Figure 23. The three-point representation of angular dependence of the average backscatter coefficient did not preserve the real drop-off observed on sleet as, by way of example, in Figure 12. There it was shown that a true specular response is indeed possible at 35 GHz. The value of σ° at 45 deg is at least 18 dB below that for nonspecular

scatter, ruling out the latter mechanism. We saw in the higher-frequency signals from sleet in Figure 12 a much stronger incoherent component in the received signal. Comparing the average levels in Figure 22 with the models, there exists still a distinctive difference of 8 dB or more at a 45-deg grazing angle, attesting to a strong specular component in the scattered signal. The melt-freeze snow averages in the same figure (the dashed lines) conform in their angular dependence much more closely to the incoherent scattering models. One may have to exempt the 35-GHz curve from this statement, since between 90 deg and 45 deg the slope of the curve is still steeper than expected from the model. Even though the sample in Figure 13 does not show a distinctive "main lobe", there is on the average a considerable contribution from a specular component at this frequency and over this type of snow. Between 45 and 15 deg, the slope of the 35-GHz line agrees well with the one calculated for volume scatter. Fitting the model curves to the measured data at the upper two frequencies yields good agreement in the angular range between 90 and 45 deg. That is, any indication of specular scatter is clearly ruled out in this angular range. The differences between expected values for volume scatter and rough-surface scatter are not significant enough to conclude which scatter mechanism is predominant above a grazing angle of 45 deg. Below 45 deg, and judging by the slope of the lines connecting the 15- and 45-deg points, volume scatter is the mechanism accounting for σ°. Of course, the lowest grazing angle considered here is not low enough to produce a really convincing result. It is well possible that contributions from both incoherent scatter mechanisms exist with comparable magnitude, making it again difficult to sort out one mechanism or the other.

Figure 23, showing the results for ET snow, is not too different in angular dependence of backscatter coefficient from Figure 22. The 35-GHz data show a behavior intermediate to sleet and MF snow, presumably because the crustal layer approaches the mirror properties of the frozen sleet. At angles below 45 deg, the line slopes down in agreement with the one postulated for volume scatter. The same is true at 98 and 140 GHz. The crossover found at 98 GHz between VV and HH curves most likely is not significant. The two different slopes that occur are still best identified with that of volume scatter. Between 45 and 90 deg, slopes measured agree with the calculation.

4.2.2 TRANSMISSION DATA

In Section 4.1 the nature of the received signal was discussed when the system operated in the transmission mode. Transmission data will be used to obtain a measure of snow attenuation at millimeter wavelengths. The analysis will be limited to determining an attenuation coefficient for perpendicular incidence. For 35 GHz, this quantity is derived directly from the transmitted signal at perpendicular

incidence. In the case of the 98- and 140-GHz data, where the signal fluctuates rapidly, the average peak transmitted signal was determined by averaging the transmitted-signal peaks measured within 5 deg on either side of perpendicular incidence. This corresponds to the procedure used to determine the average peak backscatter as a function of grazing angle.

All attenuation data from the period before the 6 February storm are grouped together in Table 5, and all data collected subsequent to that day in Table 6. In each table the date, the snow thickness, and the density are given. One column shows the average attenuation measured at each frequency. In the last column the attenuation coefficient expressed in dB per meter is given. All measurements shown in Table 5 were made in the vertical polarization mode. Following the blizzard, the attenuation was measured in both polarization modes and both are shown in Table 6. Under field conditions it is reasonable to assume a measurement accuracy for attenuation no better than 2 dB. Attenuations below this level were not used to obtain average values. A fair amount of the 35-GHz data fall into this category. They are shown in parentheses.

To provide a basis for comparison, attenuation coefficients have been calculated assuming snow to be a dielectric medium composed of ice and air. Stiles and Ulaby[18] give the attenuation coefficient through snow as

$$L = -\frac{8.68\,\pi\,\epsilon_i}{\lambda\sqrt{\epsilon_r}}\ \text{dB/m}\,, \tag{14}$$

with ϵ_r as the real part and ϵ_i the imaginary part of the dielectric constant ϵ_s of the mixture. In the snow multipath report[12] we derived the dielectric constant of snow from a mixing formula cited by Cumming.[19] Stiles and Ulaby use Wiener's[20] mixing formula referenced by Evans[21] which permits one to take internal structure of snow into consideration. If we assume the dielectric constant of air to be unity, Wiener's equation reduces to

$$(\epsilon_s - 1)(\epsilon + F) = f(\epsilon - 1)(\epsilon_s + F)\,, \tag{15}$$

18. Stiles, W.H., and Ulaby, F.T. (1980) Microwave Remote Sensing of Snowpacks, NASA Contr. Rep. 3263, Contr. NAS 5-23777.

19. Cumming, W.A. (1952) The dielectric properties of ice and snow at 3.2 centimeters, J. Appl. Phys. 23(No. 7):768-773.

20. Wiener, O. (1910) Zur Theorie der Refraktionskonstanten, Berichte, Gesellschaft d. Wiss. zu Leipzig, Math. - Phys. Klasse, 62(Hft. 5):256-277.

21. Evans, S. (1965) Dielectric properties of ice and snow; a review, J. of Glaciology, 5:773-792.

where

ϵ dielectric constant of ice,
f fractional volume occupied by ice,
F form factor, ranging from zero to infinity;
F = 2 for ice spheres.

The dielectric constant of ice, a low-loss medium, approximately relates to the real and imaginary component (n_r, n_i) of the refractive index given by Ray[11] and quoted earlier in the report as

$$\epsilon = n_r^2 + j\, 2\, n_r n_i \,. \tag{16}$$

Based on a form factor F = 2, dielectric constants of snow have been calculated from Wiener's formula at the three frequencies for average densities measured during the tests. Attenuation coefficients for the various snows and for plain ice were then derived using Eq. (14). The results are tabulated in Table 7. A comparison of experimental data in Tables 5 and 6 with the calculated ones in Table 7 makes clear that millimeter-wave attenuation through snow which apparently involves particle resonances is not described satisfactorily by the Wiener formula. Even when implementing the equation with F equal to infinity, the predicted attenuation coefficients come nowhere near the ones measured at 98 and 140 GHz. The same can be said when applying the Cumming formula.

Examining Tables 5 and 6 in more detail, one sees quite a bit of scatter in the data. However, a number of trends are discernible. First, the attenuation coefficient measured at 35 GHz through the post-blizzard snow (Table 6, ET snow) is intermediate to that measured through sleet and MF snow (Table 5). Second, this does not appear to be the case at the two higher frequencies. With the exception of 24 February, the attenuation coefficients measured at 98 and 140 GHz through ET snow are, on the whole, lower than all values obtained from sleet and MF snow. Third, it appears that the attenuation coefficient may depend on the slab thickness. In the pre-blizzard tests of Table 5, the largest values of L were measured at 98 and 140 GHz through the sleet slab of 17 January. It was also the thinnest of all the slabs tested during this period. At 35 GHz, the attenuation through this slab was too small to be considered. Also, the 98- and 140-GHz attenuation coefficients through the 6-cm slabs seem higher on the average than those through 10 to 14-cm slabs. This conclusion is strengthened by attenuation measurements performed on 24 February on the single 2.5-cm crust slab vs the others during this period of stable snow structure which had 12.7 cm thickness. The particle size and density

contained in the crust did not differ appreciably from those in the underlayer. It is not clear, if the differences in hardness between the top and lower layers suffice to make them different in terms of quantity L. The brittle portion was not investigated separately for its attenuation coefficient.

The theory of multiple scattering in optics[22] provides a reasoning for L-dependence on sample thickness. Consider a beam of photons incident upon a scattering medium. As the beam propagates into the medium, photons are scattered out of it resulting in attenuation of the beam. If the density of scatterers is high enough and the medium is thick enough, eventually some of the photons scattered out of the beam will be directed back in through multiple scattering. When this is the case, the net rate at which photons are lost out of the beam is reduced. Thus the average attenuation coefficient measured from a sample thick enough that multiple scattering is appreciable would be smaller than that measured through a thin slab where multiple scattering is negligible. A sketch of this behavior appears in Figure 25. The slope of the curve reduces from its original value in proportion to the effect that multiple scattering has as the sample thickness increases. Some steady state may be reached when the amount of power scattered back into the beam is equal to that scattered out. When this condition is reached, the slope of the curve could be due to absorption only. Conceivably, Wiener's formula is a closer match at this point.

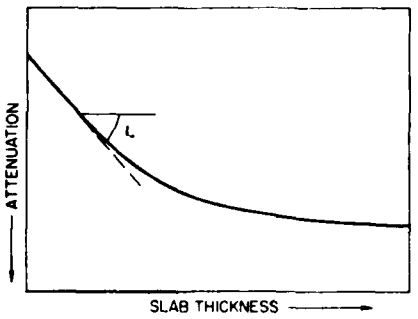

Figure 25. Hypothetical Attenuation Curve for Scattering Medium

22. Ishimaru, A. (1978) Wave Propagation and Scattering in Random Media, Vol. 2, Academic Press, New York.

Table 5. Average Attenuation Coefficient, (vertical polarization, 17 January to 2[illegible]ebruary 1978)

Date	Snow Thickness (cm)	Snow Density (g/cm^3)	Attenuation (dB)			Attenuation Coeff. (dB/m)		
			35 GHz	98 GHz	140 GHz	35 GHz	98 GHz	140 GHz
17 January	5.1	0.53	(0.1)	23	22	(2.7)	452	432
24 January	11.0	0.40	5	29	36	44	267	32[illegible]
27 January	11.0	0.26	11		24	96		215
28 January	14.0	0.31	13	28	32	90	200	231
28 January	10.0	0.31		27			272	
30 January	10.0	0.29		25	37		245	374
30 January	6.5	0.29		18	21		275	231
31 January	6.4	0.29	(0.5)		24	(8.4)		331
31 January	6.4	0.31	(0.8)	24	28	(11.8)	380	433
1 February	6.4	0.29		15			231	
2 February	12.5	0.31			37			296
2 February	6.2	0.31			21			335
6 February	11.0	0.28	6			51		
6 February	6.3	0.28	8			122		

Table 6. Average Attenuation Coefficient, (vertical and horizontal polarization, 21 February to 2 March 1978)

Date	Snow Thickness (cm)	Snow Density (g/cm^3)	Attenuation (dB)						Attenuation Coeff. (dB/m)					
			35 GHz		98 GHz		140 GHz		35 GHz		98 GHz		140 GHz	
			VV	HH	VV	HH	VV	HH	VV	HH	VV	HH	VV	HH
21 February	6.4	0.28	(0.9)						(13.6)					
21 February	12.7	0.28	(1.0)		21		21		(7.6)		169		165	
22 February	12.7	0.24	1.6)		27	18	24		(12.4)		212	139	185	
23 February	12.7	0.28	3.3	4.1			20	21	26	32			160	165
24 February	2.5	0.22	(-1.3)	(-0.3)	15	6	15	16			587	237	609	633
27 February	12.7	0.23	(1.1)	3.0	19	21	23	29	(8.8)	24	148	163	180	231
1 March	12.7	0.29	4.3	3.2	24	23	31	31	34	25	192	181	243	243
2 March	8.9	0.27	(1.2)	2.0	11	19	27	24	(13.2)	22	128	213	302	272

Table 7. Calculated Attenuation Coefficient of Snow Using Wiener Formula

Snow Condition	Density (g/cm^3)	Frequency (GHz)	Dielectric Constant		Attenuation Coeff. (dB/m)
			ϵ_r	ϵ_i	
Equitemperature Snow 21 Feb. - 2 March	0.26	35	1.37	3.5×10^{-4}	0.96
		98	1.37	2.0×10^{-4}	1.56
		140	1.37	1.2×10^{-4}	1.40
Melt-Freeze Snow 21 Jan. - 6 Feb.	0.29	35	1.42	4.1×10^{-4}	1.08
		98	1.42	2.3×10^{-4}	1.75
		140	1.42	1.4×10^{-4}	1.55
Layered Sleet and Snow 24 January	0.40	35	1.60	6.2×10^{-4}	1.56
		98	1.60	3.5×10^{-4}	2.52
		140	1.60	2.1×10^{-4}	2.28
Sleet Layer 17 January	0.53	35	1.86	9.4×10^{-4}	2.19
		98	1.86	5.3×10^{-4}	3.53
		140	1.86	3.2×10^{-4}	3.16
Ice	1.00	35	3.17	3.2×10^{-3}	5.70
		98	3.17	1.8×10^{-3}	9.10
		140	3.17	1.1×10^{-3}	8.20

In line with the foregoing discussion, a least-mean-square curve-fit analysis of the attenuation data was performed. At each frequency the pre-blizzard (melt-freeze) and post-blizzard (equitemperature) snow were considered separately. Linear and quadratic curve fits were made based on a subjective decision as to which best matched the data. In the case of 35 GHz, straight-line fits proved to be best. A parabolic fit was selected at the higher frequencies. For all data sets, zero attenuation for zero slab thickness was included as one input data point to the curve-fitting analysis. The results are shown in Figures 26, 27, and 28 for 35, 98, and 140 GHz, respectively.

At 35 GHz (Figure 26) two things are apparent. First, the attenuation through melt-freeze snow exceeds by a factor of two or three that through equitemperature snow. Second, there is larger scatter in the MF data. In the case of ET snow, the attenuation measured for vertical and horizontal polarization have been plotted together. This assumes polarization independence of attenuation at perpendicular incidence. An average of all the data at each frequency bears this out.

For 98 GHz (Figure 27), one sees an increase in attenuation over that for 35 GHz. The ordinate scale has been compressed to one-half that used for the 35-GHz data. Again, the attenuation through MF snow is greater than that through ET snow. The parabolic curve fit to the melt-freeze data is quite good and shows a leveling-off as the slab thickness increases. On the other hand, there is a large spread between the vertically and horizontally polarized measurements through

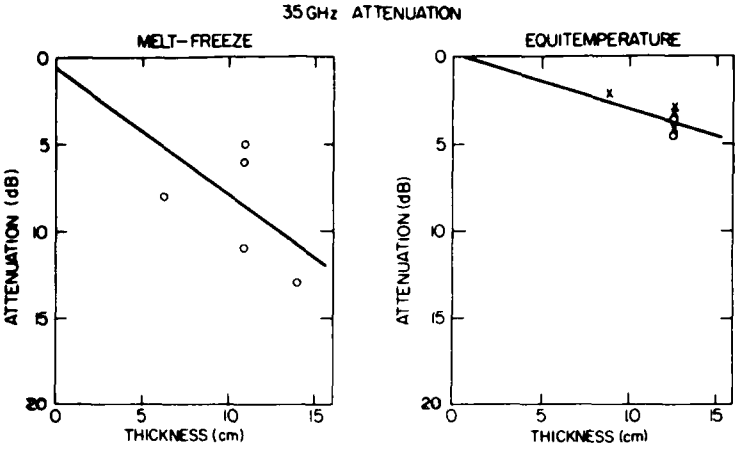

Figure 26. Attenuation vs Slab Thickness at 35 GHz, (polarizations vertical o, horizontal x)

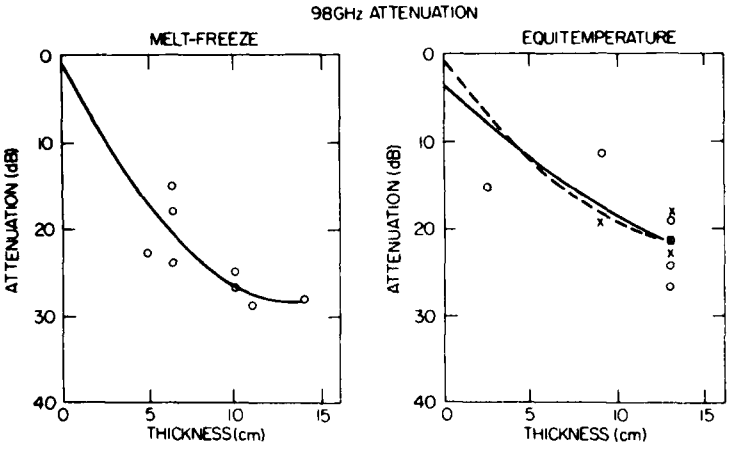

Figure 27. Attenuation vs Slab Thickness at 98 GHz, (polarizations vertical o, horizontal x)

ET slabs. The curve fit to these data is correspondingly poorer. As the horizontally polarized data look better, a parabola has been fitted to these points alone (the dashed curve in Figure 27). At 140 GHz (Figure 28), the attenuation coefficient through MF snow is again seen to be greater than through ET snow.

Attenuation coefficients taken from the slope of the straight lines at 35 GHz and from the initial slopes of the parabolas at 98 and 140 GHz are presented in Table 8.

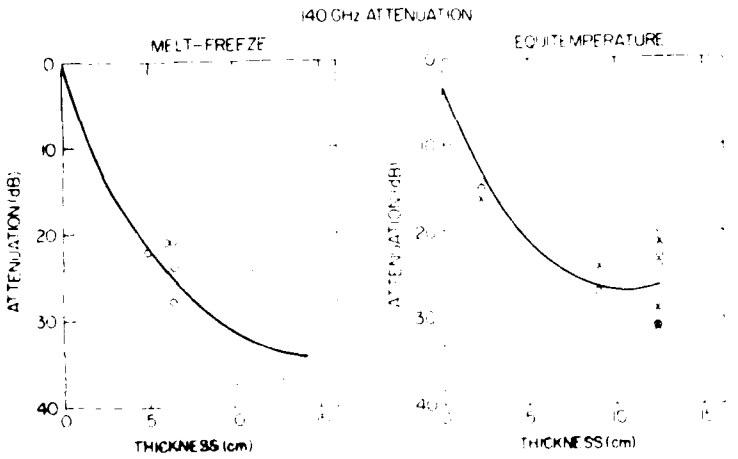

Figure 28. Attenuation vs Slab Thickness at 140 GHz, (polarizations vertical o, horizontal x)

At 35 GHz, the attenuation coefficient measured through MF snow is more than double that through ET snow. There is a sharp increase in L as the frequency increases to 98 GHz. Again, the value through MF snow is greater than that through ET snow. The value pertaining to horizontal polarization alone is shown in parentheses. At 140 GHz, the attenuation coefficient has become even greater. At this frequency it is essentially equal for both types of snow.

Table 8. Attenuation Coefficient vs Frequency, (initial slope of curves fitted to data)

Frequency (GHz)	Attenuation Coefficient (dB/cm)	
	Melt-Freeze Snow	Equitemperature Snow
35	74	29
98	413	183(313)
140	506	495

If multiple scattering is much weaker at 35 GHz (judging from the absence of modulation on the 35-GHz data compared to the higher frequencies) then thicker samples would be needed to obtain results at this frequency comparable to the ones at the higher frequencies. To prove this, additional measurements are required. Measurements of attenuation should preferably be made on a series of snow slabs, each of increasing thickness but otherwise unchanging characteristics.

4.3 Comparison With Other Results

In the report discussing the in-situ data,[14] backscatter coefficients in the sample and in-situ modes are compared with the results obtained by other researchers. In this report, discussion will be limited to a comparison of the slab backscatter data with the in-situ data. When operating in the sample mode it is implied that cutting and removing the slab from the snow cover does not perturb its scattering and attenuation properties. The 3-dB beamwidths of the three transmitting antennas are narrow enough so that only a portion of the slab is illuminated. Under this condition, the finite slab appears equal to one infinite in size. Further, the slab must be thick enough so that the snow/air interface on its underside plays no role in the strength of the scattered signal. The validity of these assumptions is tested by comparing backscatter coefficients from both types of measurements. Ideally, comparisons should be made on the same day and on the same snow. This was impossible due to the complexity of equipment reconfiguration from one mode to the other. Sample measurements were therefore carried out during the earlier part of the season, in-situ measurements during the later part. Sample data gathered in February and early March are compared here with in-situ data gathered in March.[14] Sample data represent ET snow conditions. These conditions persisted some time into the in-situ measurement period, making the two types more comparable. The in-situ program lasted through the remainder of the winter, including the late diurnal melt-freeze cycles. Hence, some differences in the results may be attributable to differences in the snow. In general, the two modes of operation produced similar output. Averages of σ° obtained in the two modes are shown in Figures 29, 30, and 31, one figure for each frequency. The agreement between the sample and in-situ measurements is best at 140 GHz, with differences ranging to no more than 3 dB. The sample data show somewhat higher levels of σ°_{VV} than σ°_{HH}. This is not repeated in the in-situ data and we conclude that a polarization dependence of the like-polarized backscatter coefficient cannot be claimed from the available results. This fact is corroborated by what is seen at the two lower frequencies in Figures 29 and 30. Averaging over all like-polarized σ° at 140 GHz (Figure 31) leads to a 2.1-dB difference between 90 and 45-deg levels, and to a 9.6-dB difference between 90- and 15-deg levels. This matches with the expected drop-off for incoherent scatter. Cross-polarized backscatter is significant and within 3 dB of the like-polarized values at all angles for both types of measurement.

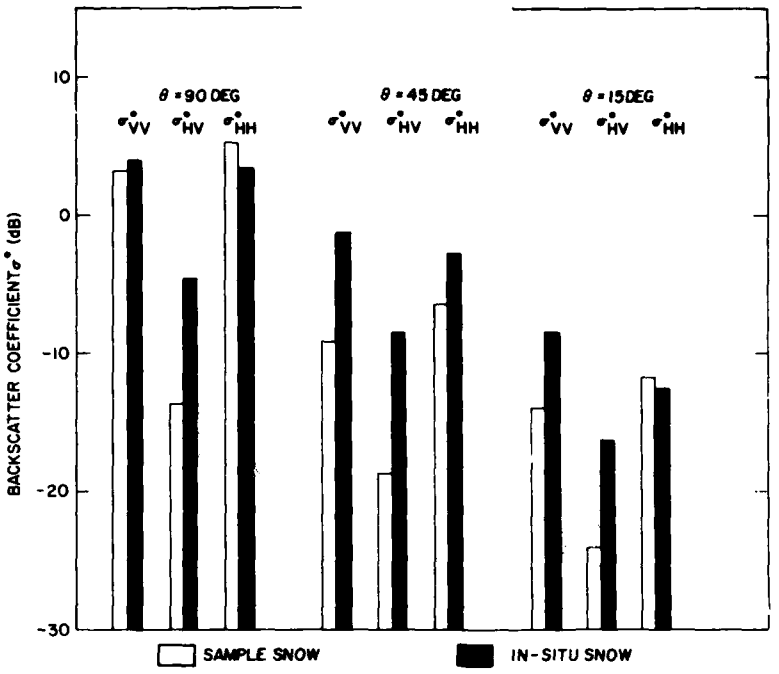

Figure 29. Comparison of Sample and In-situ Data at 35 GHz

Almost the same good agreement is found for 98-GHz results. There is a slight indication of a level drop between 90 and 45 deg, corresponding to a stronger specular component. The difference between like- and cross-polarized σ° is also larger, of the order of 4 to 5 dB. The tendency of the in-situ data to exceed the sample data is almost consistent for all types of σ° and for all angles. Based on previous reasoning, and in consideration of attenuation coefficients measured at this frequency, we still feel that differences must be of a statistical nature as implied at 140 GHz and not due to the limited depth of the slabs.

Conditions are distinctly different at 35 GHz. Here we note a characteristic and systematic difference of 8 to 10 dB between the cross-polarized backscatter coefficient measured on samples and on the ground. We interpret the difference in two ways. Path attenuation through snow is low enough so that contributions from the back side of the slab definitely contribute to the cross-polarized signal. Due to generally greater snow depth on the ground, more scattering occurs in the in-situ case. There is further the fact that the ground below the snow reflects the 35-GHz signal which upon reflection illuminates more snow particles for more cross-polarized backscatter. The like-polarized data can be used to support

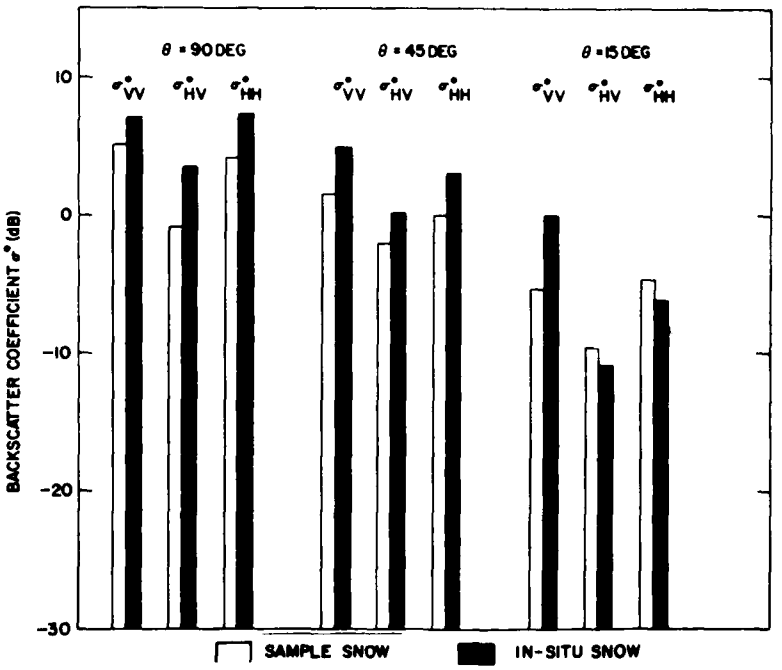

Figure 30. Comparison of Sample and In-situ Data at 98 GHz

this argument. At perpendicular incidence, the snow surface is generally smooth enough at 35 GHz to cause a strong specular response, equal to or higher than the noncoherent response. No substantial snow depth is required to generate this signal and correspondingly σ°_{VV} and σ°_{HH} are comparable for the sample and in-situ data. It is at the lower grazing angles that the depth of the snow comes to bear on the strength of the like-polarized σ°. The sample data show the characteristic specular response seen previously in this report. That is, from the very high perpendicular return at 90 deg there is an abrupt lowering at 45 deg to incoherent signal levels from the slab which is not thick enough to represent infinite snow depth at this frequency. Whether or not an average snow depth of 30 cm found during in-situ measurements does this is debatable. There is significantly higher like-polarized backscatter than observed on samples. This explanation is supported, if one assumes that at lower grazing angles reflection off the ground becomes fairly effective, with the ground-reflected signal again producing like-polarized backscatter off the snow cover. In summary, it appears to be safe to conclude that at 98 and 140 GHz the sample measurement technique represents in-situ conditions quite well. At 35 GHz, the scatter levels are lower than what can be expected for

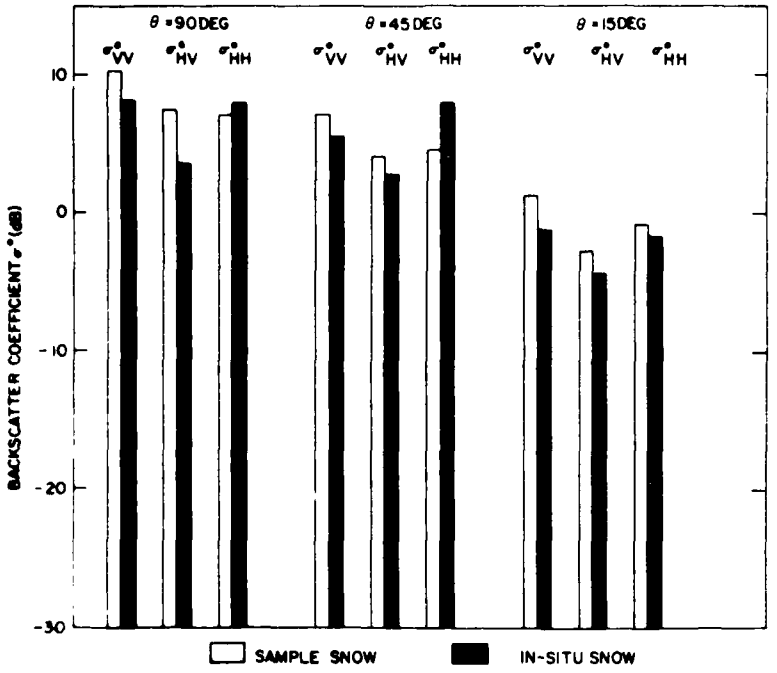

Figure 31. Comparison of Sample and In-situ Data at 140 GHz

in-situ snow of great depth. In many practical situations the snow depth is limited. Under these conditions the slab data may be quite representative at this frequency.

A review of the subject of microwave attenuation through snow cover is contained in the report by Stiles and Ulaby.[18] In addition to attenuation data they collected at 35.6 GHz, they discuss attenuation measurements made by Currie et al[7] at 35 and 95 GHz and measurements made by Battles and Crane[23] at 35 GHz using snow produced in the laboratory. Figure 32, taken directly from the University-of-Kansas report shows the procedure of snow attenuation measurements. A composite layer is formed by stacking slabs from the snow cover to stepwise increase the thickness of the layer. The results of these measurements are shown in Figure 33. This figure has also been taken from the Stiles and Ulaby report. Earlier it was suggested that at 35 GHz our slabs were not thick enough to show a nonlinear dependence of attenuation upon slab thickness. This is borne out by the Stiles and Ulaby data for dry snow. A flattening in the attenuation curve in Figure 33 appears

23. Battles, J.W., and Crane, D.E. (1966) Attenuation of Ka-Band Energy by Snow and Ice, U.S. Naval Ordnance Lab., NOLC Rep. 670, Corona, California, AD 638303.

only when the slab thickness approaches 40 cm. During these measurements snow was simply characterized as dry, wet, or very wet. It should be noted that the attenuation coefficient measured by us through ET snow agrees fairly well with the average slope before the flattening of the curve shown for dry snow in Figure 33.

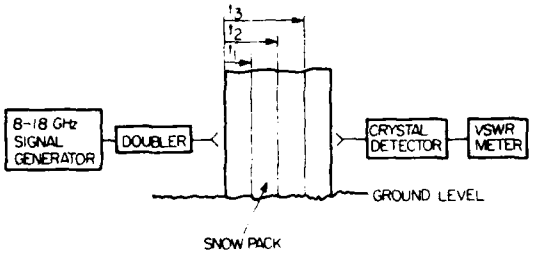

Figure 32. Diagram Illustrating the Stiles and Ulaby[18] Attenuation Measurement Through Layers of Snow at 35.6 GHz

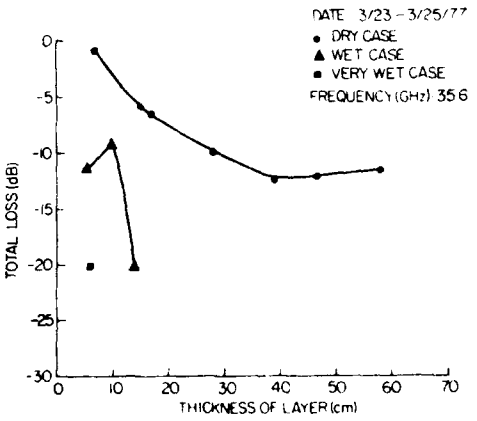

Figure 33. Path Loss Measured by Stiles and Ulaby[18] as a Function of Snow Thickness

Currie's et al[7] experimental arrangement consisted of two truck-mounted pulse radars reflecting signals off a 10-in. corner reflector. The two-way attenuation through snow was measured by placing slabs in front of the corner reflector and measuring the radar return. A reference signal was obtained by raising the corner reflector above the snow slab and then measuring the return. Their attenuation data are given in Table 9. Snow properties in their report are not described in any

greater detail than that listed in Table 9. It is therefore impossible to make a detailed comparison of their data and ours. On the one occasion that they made simultaneous measurements at 35 and 95 GHz, the values of the attenuation coefficient they obtain are in rough agreement with those we measured through MF snow. The attenuation coefficient on 15 April at 35 GHz seems anomalously high. As we have seen in our data, rotation of the snow slab results in a random fluctuation of the transmitted signal. It is conceivable that this high value is due to critical positioning of the slab. Currie et al measured an increase in the attenuation coefficient at 35 GHz through wet snow but essentially no change at 95 GHz. We did not measure attenuation through wet snow, but as part of our in-situ measurements we did determine the effect of snow wetness upon the backscatter coefficient. We found a decrease in the effect of free water upon the backscatter signal as the frequency increases.

Table 9. Loss Measurements at 35 GHz and 95 GHz by Currie et al[7]

Date	Time	Frequency (GHz)	Polariz.	Snow Thickness (cm)	Snow Condition	Loss (dB)	Atten. Coeff. (dB/m)
14 April 1976	1529	95	HH	6.0	Wet	30	250
15 April 1976	0742	35	HH	4.6	Frozen Snow Crust	21	228
16 April 1976	0635	35	HH	5.0	Frozen Snow Crust	5	50
		95	HH	5.0	Frozen Snow Crust	30	300
	0639	35	VV	5.0		10	100
	0720	35	HH	3.5		3	43
	0723	35	VV	3.5		7	100
	0746	35	VV	3.5	Melting Snow Crust	14	200
	0748	35	HH	3.5		11	157

Battles and Crane[23] used an interferometer to measure attenuation at 35 GHz through snow and ice manufactured in an environmental chamber. The objective of their study was to determine the effect on attenuation of the variation of snow density at a fixed temperature. All tests were made at -25°C. Their findings are

presented in Table 10. They claim their loss measurements are accurate to within 0.5 dB. Their "snow" was produced by spraying a fine mist of cold water or hot water into the cooled environmental chamber. By varying the water temperature, pressure, and chamber temperature they were able to produce snow particles of varying sizes. Snow particles produced in this way most closely resemble small hail or sleet particles. The size of the particles ranged from 0.3 mm for the fine snow up to almost 2 mm for the large ice crystals. Samples composed of large ice crystals are similar to the MF slabs used in our tests. In this case, the attenuation coefficient (65.7 dB/m) reported by Battles and Crane is in rough agreement with ours (average 74 dB/m). They also show the effect of increasing the density of the snow by packing it. Scattering should decrease and consequently attenuation should decrease. Also, if the size of the particles is small compared to the wavelength, scattering and thus attenuation should decrease likewise. This is true for the fine, loose snow where the ratio of particle diameter to wavelength is approximately 0.03. The attenuation coefficient they determined through ice is four times higher than the calculated value in Table 7. It is not known if their ice slab was free from air bubbles which would tend to increase attenuation due to scattering from the bubbles.

Table 10. Loss Caused by Snow and Ice at 35 GHz, (Battles and Crane[23])

Type	Thickness (cm)	Density (g/cm^3)	Loss (dB)	Atten. Coeff. (dB/m)
Fine loose snow	14.0	0.20	2.5	17.9
Locally packed loose snow	14.0	0.33	7.2	51.4
Large ice crystals	14.0	0.39	9.2	65.7
Packed snow	14.0	0.47	1.4	10.0
Ice	5.1	0.92	1.2	23.4

5. CONCLUSIONS

Metamorphic snow in the frozen state represents a medium of low-loss, densely packed particles of resonant size in the millimeter wave region. Sometimes, depending on the process of development, internal bonds are strong enough to approximate an ice layer of relative smoothness in terms of wavelength. It was the purpose of this report to determine scattering and attenuation characteristics of the

medium at the atmospheric-window frequencies of 35, 98, and 140 GHz. Measurements were obtained on slabs of snow which could be conveniently removed from natural snow cover. This technique is almost mandatory in order to obtain attenuation data, but proved to be advantageous also in studying backscatter and bistatic scatter phenomena. One major advantage of the experimental system developed for the program is its ability to provide contiguous coverage in grazing angle. Care was taken to contain the area of wave/snow interaction within the lateral extent of the slab and to keep the scatterers within the far field of the antennas used. Snow depth proved to be one critical parameter that could not be fully satisfied at 35 GHz, the lowest frequency investigated. Significant contributions from snow depths greater than the slab thickness could be expected as a comparison with similar measurements on in-situ snow reveals. Slab thickness was no problem at the higher frequencies, 98 and 140 GHz.

Two parameters were investigated regarding their dependence on grazing angle to aid in the interpretation of the received signal and to reveal the spatial arrangement of scatterers. These were the number of fluctuations due to phasing observed per deg slab rotation, and the drop-off in signal strength as the grazing angle reduces. Neither provided unambiguous evidence as to the scatter mechanisms involved. It was found that reflection from a smooth dielectric interface, scattering from a rough surface, and scattering from a volume of particles were generally not observable individually. The one exception, 35-GHz scatter from an ice-like surface where specular reflection predominates at perpendicular incidence, is somewhat in doubt because deeper snow might have resulted in a more substantial volume scatter contribution. Apart from diffraction effects, which must be considered edge effects on the fluctuation-rate measurement, neither of the three scatter mechanisms could be singled out clearly on the basis of angular changes in the number of fluctuations observed. This is not necessarily a detriment but simply an indication of the complexity of the medium which interacts with millimeter waves in a mixed mode. Thus, it is partially reflecting in a specular manner if snow composition, grazing angle, and frequency are appropriate, and otherwise, the surface layer or deeper lays are scattering incoherently, again depending on the three parameters above. It must be noted that incoherent signal levels can be quite comparable to coherent ones.

In order to assess the influence of snow structure on scattering and attenuation, three types of metamorphic snow were identified, related to time periods of the progressing winter season. Distinctions were made primarily in line with meteorological classifications. The measured data suggest some systematic differences in millimeter wave interaction with the three snow types specified. For a system designer they might be largely unimportant. A convincing difference between

vertical and horizontal-polarization results could not be established at any frequency or any grazing angle investigated. This applies to backscatter and attenuation. Cross-polarized backscatter was surprisingly high, reaching levels within several dB of like-polarized backscatter, when the incoherent scatter mechanism prevailed. When specular scatter dominated, the cross-polarized component was low.

At 90 deg grazing angle, average backscatter coefficients were measured at 35, 98, and 140 GHz: off sleet 11, 9, 11.5 dB, off MF snow 3, 8, 9.5 dB, off ET snow 6, 4.5, 9 dB, off ET snow (cross-polarized) -13, -1, 7.5 dB. At 15 deg grazing angle, average backscatter coefficients were measured at 35, 98, and 140 GHz: off sleet -14, -6, -3 dB, off MF snow -11, -1.5, -0.5 dB, off ET snow -13, -4.5, 0.5 dB, off ET snow (cross-polarized) -24, -9.5, -3 dB. The attenuation coefficient at 90 deg penetration into the slab measured at 35, 98, and 140 GHz: through MF snow 74, 413, and 506 dB/m and through ET snow 29, 183 (318) and 495 dB/m.

References

1. Suits, G.H., and Guenther, B.D. (1978) Targets and Backgrounds, U.S. Army MIRADCOM, Tech. Rep. T-78-71.

2. Ulaby, F.T., Stiles, W.H., Dellwig, L.F., and Hanson, B.C. (1977) Experiments on the radar backscatter of snow, IEEE Trans. on Geoscience and Electronics, GE-15(No. 4):185-189.

3. Stiles, W.H., Hanson, B.C., and Ulaby, F.T. (1977) Microwave Remote Sensing of Snow, Experiment Description and Preliminary Results, U. of Kansas RSL Tech. Rep. 340-2.

4. Ulaby, F.T., and Stiles, W.H. (1978) The Active and Passive Microwave Response to Snow Parameters. Part I: Wetness Part II: Water Equivalent of Dry Snow, U. of Kansas RSL Tech. Rep. 340-2.

5. Ellerbruch, D.A., Little, W.E., Boyne, H.S., and Bachmann, D.D. (1977) Microwave Characteristics of Snow, Western Snow Conf. 45th Ann. Mtg., Albuquerque, New Mexico.

6. Hoekstra, P., and Spanogle, D. (1972) Backscatter from snow and ice surfaces at near incident angles, IEEE Trans. on Ant. and Prop., AP-20(No. 6):788-790.

7. Currie, N.C., Teal, J.R., Jr., Dyer, F.B., and Ewell, G.W. (1977) Radar Millimeter Backscatter Measurements From Snow, AFATL-TR-77-4.

8. Currie, N.C., Lewinsky, D.J., Applegate, M.S., and Hayes, R.D. (1977) Radar Millimeter Backscatter Measurements, Vol. I: Snow and Vegetation, AFATL-TR-77-92.

9. Ulaby, F.T., Fung, A.K., and Stiles, W.H. (1978) Backscatter and Emission of Snow: Literature Review and Recommendations for Future Investigations, U. of Kansas RSL Tech. Rep. 369-1.

10. Trebits, R.N., Hayes, R.D., and Bomar, L.C. (1978) Millimeter wave reflectivity of land and sea, Microwave J. 21(No. 8):49-53.

11. Ray, P.S. (1972) Broadband complex refractive indices of ice and water, Appl. Optics 11(No. 8):1836-1844.

12. Lammers, U.H.W., and Hayes, D.T. (1980) Multipath Propagation Over Snow at Millimeter Wavelengths, In-House Rep. RADC-TR-80-54, AD A087747.

13. Clapp, R.E. (1946) A Theoretical and Experimental Study of Radar Ground Return, Rep. 1024 Rad. Lab. MIT, Cambridge, Massachusetts.

14. Hayes, D.T., Lammers, U.H.W., and Marr, R.A. (1981) Scattering From Snow Background at 35, 98, and 140 GHz, RADC-TR (to be published).

15. Perla, R.I., and Martinelli, M., Jr. (1976) Avalanche Handbook, Agriculture Handbook 489, U.S. Dept. of Agr., Forest Service.

16. Stratton, J.A. (1941) Electromagnetic Theory, McGraw-Hill, New York.

17. Herman, B.M., and Battan, L.J. (1961) Calculations of Mie backscattering of microwaves from ice spheres, Quart. J. of the Roy. Met. Soc. 87:223-230.

18. Stiles, W.H., and Ulaby, F.T. (1980) Microwave Remote Sensing of Snowpacks, NASA Contr. Rep. 3263, Contr. NAS 5-23777.

19. Cumming, W.A. (1952) The dielectric properties of ice and snow at 3.2 centimeters, J. Appl. Phys. 23(No. 7):768-773.

20. Wiener, D. (1910) Zur Theorie der Refraktionskonstanten, Berichte, Gesellschaft d. Wiss. zu Leipzig, Math.-Phys. Klasse, 62(Hft. 5):256-277.

21. Evans, S. (1965) Dielectric properties of ice and snow; a review, J. of Glaciology, 5:773-792.

22. Ishimaru, A. (1978) Wave Propagation and Scattering in Random Media, Vol. 2, Academic Press, New York.

23. Battles, J.W., and Crane, D.E. (1966) Attenuation of Ka-Band Energy by Snow and Ice, U.S. Naval Ordnance Lab., NOLC Rep. 670, Corona, California, AD 638303.

Appendix A

Snow Data

Physical parameters of the snow cover, from which snow slabs were cut, are presented in this appendix. One combination table/diagram is given for every day on which millimeter-wave measurements were conducted (Tables A1 through A20). The data characterize the snow at the time the slabs were cut. A standard form of presentation has been used. The vertical scale at the center of the form gives the height above ground. Any snow parameter indicated on the form at this height is pertaining to this particular height. The stratigraphy of the snow cover is shown by horizontal lines drawn between the left edge of the form and the height scale. Most of the column headings are self-explanatory. The "Layer" column normally contains a one-word description of the layer such as hard, icy, brittle, and so on. In the "Density" column, a tick mark is placed to show the height at which the measurement was made. The air temperature, indicated by the ⊕ symbol on the temperature plot, was obtained at a position just above the surface of the snow. Under "Comments" is placed such information as surface hardness, weather data, data on the history of the snow, and in some cases additional data on the stratigraphy of the snow. The snow was completely frozen at the time the test slabs were cut. No melting occurred during the tests. Free-water content is therefore not listed on the form.

Table A1. Physical Parameters of Snow Cover 16 January 1978

LAYER	GRAIN TYPE	GRAIN SIZE (mm)	DENSITY (g/cm^3)	HEIGHT (cm)	TEMPERATURE DEG C (0, -5, -10, -15)	COMMENTS
Ice 1 mm thick				40, 35, 30, 25, 20, 15	⊕	Average surface hardness: 20,000 g/cm^2. Snow cover was deposited on 14 January. Sleet fell at times during storm and storm ended as freezing rain. Top 5 cm of snow cover was a hard layer composed entirely of spherical grains whose mean diameter was 2 mm. Lower 10 cm was composed of 1 mm grains, among which 2 mm spherical ice grains were dispersed. Spherical particles are due to sleet and freezing rain. Maximum temperature during day was -4°C. Day was clear and calm.
Hard	Spherical	1 to 3	0.57			
Loose Granular	Irregular	1		10, 5, 0		

Table A2. Physical Parameters of Snow Cover 17 January 1978

LAYER	GRAIN TYPE	GRAIN SIZE (mm)	DENSITY (g/cm^3)	HEIGHT (cm)	TEMPERATURE DEG C	COMMENTS
Ice 1 mm thick				40 35 30 25 20 15	0 −5 −10 −15	
Hard	Spherical	1 to 3	0.53	10		Cloudy day. Air temperature did not rise above -4°C.
Loose Granular	Rounded	1	0.29	5 0		

Table A3. Physical Parameters of Snow Cover 19 January 1978

LAYER	GRAIN TYPE	GRAIN SIZE (mm)	DENSITY (g/cm^3)	HEIGHT (cm)	TEMPERATURE DEG C	COMMENTS
1 mm Ice				40	0 -5 -10 -15	Average surface hardness: 5000 g/cm^2.
Hard to Brittle	Irregular	1	0.38	35		Top layer is new snow which fell on 18 January. Precipitation turned into rain before ending.
1 mm Ice				30		Day was clear. High temperature reached during day was -2°C.
Hard	Spherical	1 to 3	0.53	25		Densities were not measured for lower two layers. Values given are those measured on 17 January.
Brittle	Rounded	1	0.29	20		
				15		
				10		
				5		
				0		

Table A4. Physical Parameters of Snow Cover 23 January 1978

LAYER	GRAIN TYPE	GRAIN SIZE (mm)	DENSITY (g/cm^3)	HEIGHT (cm)	TEMPERATURE DEG C	COMMENTS
					0 −5 −10 −15	
New snow of 20 Jan.	Columns Many have begun to meta-morphose	1 mm in length	0.28	80 70 60 50 40 30		Average surface hardness: 120 g/cm^2.
			0.19			
Hard	Irregular	1 to 2	0.43	20		
Hard	Spherical shapes disappearing	2 to 3		10		
Granular	Rounded	1	0.36	0		

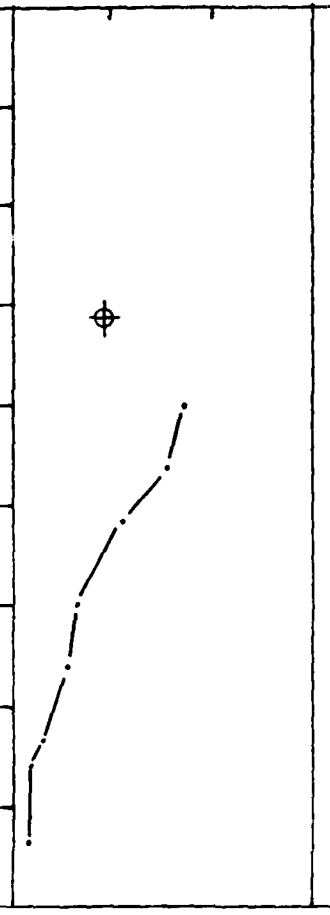

Table A5. Physical Parameters of Snow Cover 24 January 1978

LAYER	GRAIN TYPE	GRAIN SIZE (mm)	DENSITY (g/cm^3)	HEIGHT (cm)	TEMPERATURE DEG C (0, -5, -10, -15)	COMMENTS
				40		
				35		
				30		
				25		
				20		
				15		Sample was cut for use on 19 January. It lay outdoors and was covered with snow during the storm of 20 January.
20 Jan. Columns	snow and irregular shaped grains			10		
18 Jan. Irregular rounded	snow grains 1 to 2 mm			5		
14 Jan. Spherical particles	snow 2 to 3 mm			0		

Table A6. Physical Parameters of Snow Cover 27 January 1978

LAYER	GRAIN TYPE	GRAIN SIZE (mm)	DENSITY (g/cm^3)	HEIGHT (cm)	TEMPERATURE DEG C	COMMENTS
				0 −5 −10 −15		
				40		
Snow grains bonded together to form brittle structure	Melt-freeze meta-morphism present due to rain on 25 and 26 January	1	0.26	35 30 25 20 15 10		Average surface harness: 2200 g/cm^2. Rain storm of 26 January caused cusp-shaped depressions to be formed in snow surface. Depressions are about 1 cm deep and about 5 cm in diameter, 11 were counted per meter.
Solid and hard				5 0		

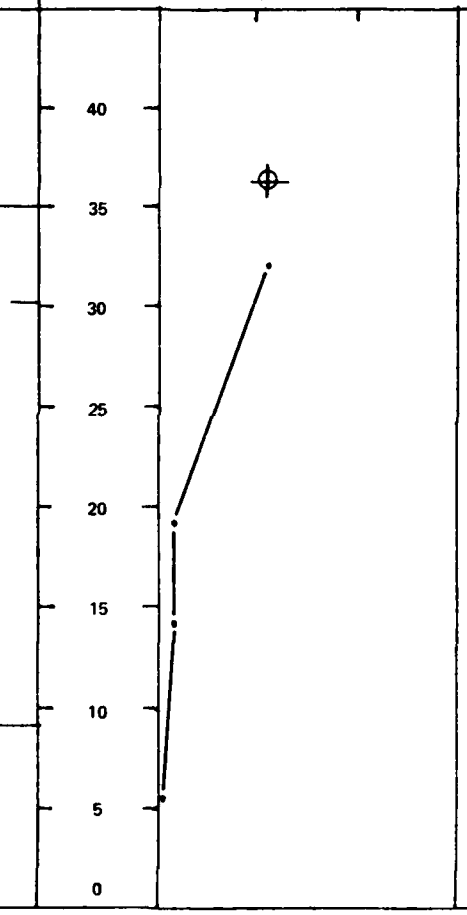

Table A7. Physical Parameters of Snow Cover 28 January 1975

LAYER	GRAIN TYPE	GRAIN SIZE (mm)	DENSITY (g/cm^3)	HEIGHT (cm)	TEMPERATURE DEG C (0, -5, -10, -15)	COMMENTS
				40		
				35		
	Irregular	1	0.31	30		Average surface hardness: 570 g/cm^2.
				25		Average hardness of middle layer: 5667 g/cm^2.
Ice				20		Snow grain condition in all layers is clearly the result of melt-freeze metamorphism. Snow grains are seen to be composed of clear ice when examined with a magnifying glass.
	Irregular	1 to 3	0.38	15		Air temperature did not rise above 0°C during tests. Sky was cloudy.
Ice						
	Irregular	1 to 2	0.36	10		
				5		
				0		

Table A8. Physical Parameters of Snow Cover 30 January 1978

LAYER	GRAIN TYPE	GRAIN SIZE (mm)	DENSITY (g/cm^3)	HEIGHT (cm)	TEMPERATURE DEG C (0, −5, −10, −15)	COMMENTS
				40, 35, 30		
	Irregular	1	0.28	25, 20		Average surface hardness: 333 g/cm^2. Average hardness of middle layer: 5778 g/cm^2. Melt-freeze metamorphism present in all layers. Air temperature did not rise above 0°C during tests. Sky was clear.
Ice				15		
	Irregular	1 to 2	0.39	10		
Ice						
	Irregular	1		5, 0		

Table A9. Physical Parameters of Snow Cover 31 January 1978

LAYER	GRAIN TYPE	GRAIN SIZE (mm)	DENSITY (g/cm^3)	HEIGHT (cm)	TEMPERATURE DEG C	COMMENTS
					0 −5 −10 −15	
				40		
				35		
				30		
Very brittle to touch	Irregular	1	0.29	25		Average surface hardness: 300 g/cm^2.
				20		Average hardness of snow below first ice layer: 3000 g/cm^2.
Ice						
	Irregular	2	0.31	15		In all layers grains were closely bonded forming particles as large as 5 mm in diameter.
				10		Day was sunny and calm. Air temperature did not rise above -6°C.
Ice						
	Irregular	2		5		
				0		

Table A10. Physical Parameters of Snow Cover 1 February 1978

LAYER	GRAIN TYPE	GRAIN SIZE (mm)	DENSITY (g/cm^3)	HEIGHT (cm)	TEMPERATURE DEG C (0, -5, -10, -15)	COMMENTS
				40		
				35		
				30		Average surface hardness: 550 g/cm^2.
Brittle	Irregular	> 1 More bonded together than on 31 Jan.	0.29	25		Average hardness of snow below first ice layer: 3500 g/cm^2.
				20		Snow conditions essentially unchanged since 31 January.
Ice						In all layers grains were closely bonded forming particles as large as 5 mm in diameter.
Quite hard	Irregular	2	0.38	15		Day was sunny and calm. Air temperature did not rise above -6°C.
				10		
Ice						
				5		
	Irregular	2		0		

Table A11. Physical Parameters of Snow Cover 2 February 1978

LAYER	GRAIN TYPE	GRAIN SIZE (mm)	DENSITY (g/cm^3)	HEIGHT (cm)	TEMPERATURE DEG C (0, -5, -10, -15)	COMMENTS
				40		
				35		
				30		Average surface hardness: 533 g/cm^2.
Brittle	Irregular	> 1	0.31	25		Average hardness of snow below first ice layer: 6000 g/cm^2.
				20		Snow conditions essentially unchanged since 31 January.
Ice						In all layers grains were closely bonded forming particles as large as 5 mm in diameter.
Hard	Irregular	2	0.35	15		Sky was overcast during most of day. Air temperature did not rise above -6°C.
				10		
Ice						
	Irregular	2		5		
				0		

Table A12. Physical Parameters of Snow Cover 4 February 1978

LAYER	GRAIN TYPE	GRAIN SIZE (mm)	DENSITY (g/cm^3)
Brittle	Irregular	> 1	0.28
Ice			
Hard	Irregular	2	0.27
Ice			
	Irregular	2	

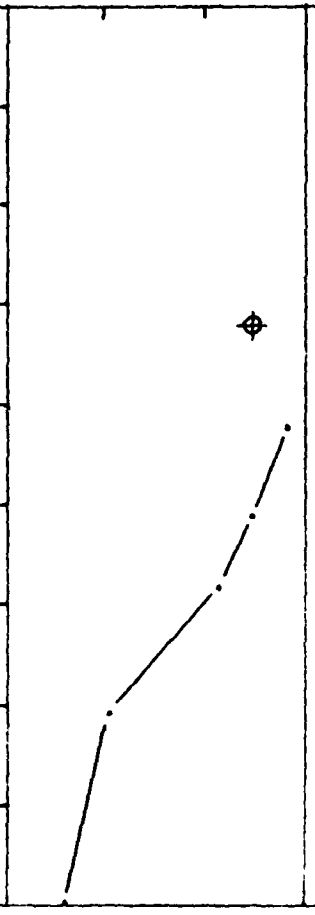

COMMENTS

Average surface hardness: 733 g/cm^2.

Average hardness of snow below first ice layer: 3667 g/cm^2.

Snow conditions essentially unchanged since 31 January.

In all layers grains were closely bonded forming particles as large as 5 mm in diameter.

Sky was clear during tests. Air temperature did not rise above -11°C.

Table A13. Physical Parameters of Snow Cover 21 February 1978

LAYER	GRAIN TYPE	GRAIN SIZE (mm)	DENSITY (g/cm^3)	HEIGHT (cm)	TEMPERATURE DEG C (0, −5, −10, −15)	COMMENTS
Crust	Rounded			80		Average surface hardness: 4333 g/cm^2.
Snow of 6 Feb.	Rounded	0.5	0.28	70		Hardness measured from side (excluding crust): 533 g/cm^2.
				60		NOTE ON SURFACE CRUST: Most of the 1-mm grains were bonded together. The average size of the bonded particles was 2 mm. Some were as large as 5 mm.
				50		BELOW CRUST: Grains were very loosely bonded or not bonded at all.
				40		Day was sunny and calm. Air temperature did not rise above -2°C.
			0.35	30		
Snow of 20 Jan.				20		
18 Jan. and earlier snow				10		
				0		

Table A14. Physical Parameters of Snow Cover 22 February 1978

LAYER	GRAIN TYPE	GRAIN SIZE (mm)	DENSITY (g/cm^3)	HEIGHT (cm)
Crust	Rounded	1		
Snow of 6 Feb.	Rounded	1	0.24	80
				70
				60
				50
				40
			0.31	30
Snow of 20 Jan.				20
18 Jan. and earlier snow				10
				0

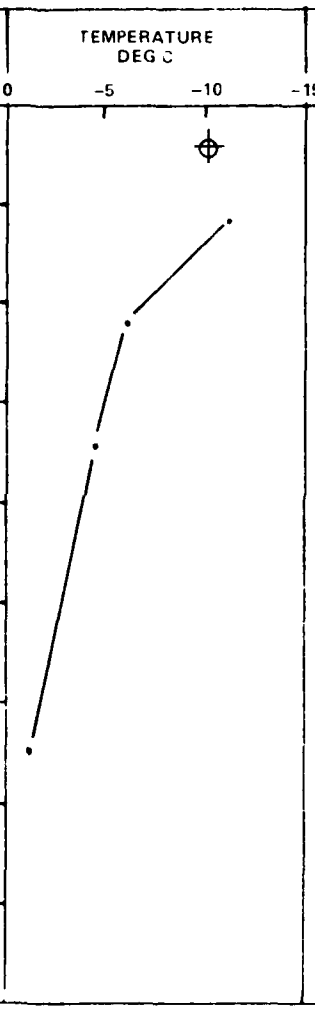

COMMENTS

Average stability index 6833 $g \cdot cm^{-2}$.

NOTE ON SURFACE CRUST:
As noted on 21 Feb., most of the 1 mm grains were bonded together. The largest size of the bonded particles was 2 mm. Some were as large as 5 mm.

BELOW CRUST:
Grains were very loosely bonded or not bonded at all.

Day was sunny and calm. Air temperature did not rise above -5°C.

Table A15. Physical Parameters of Snow Cover 23 February 1978

LAYER	GRAIN TYPE	GRAIN SIZE (mm)	DENSITY (g/cm^3)
Crust	Rounded	1	
Snow of 6 Feb.	Rounded	1	0.28
			0.34
Snow of 20 Jan.			
18 Jan. and earlier snow			

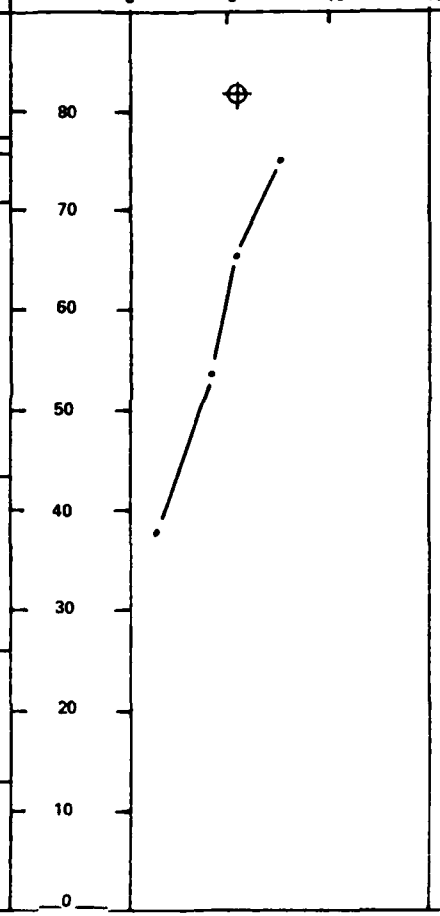

COMMENTS

Average surface hardness: 3666 g/cm^2.

Snow crust and snow below crust was unchanged from data of 22 Feb. as to particle size.

Day was sunny and calm until 11:00 when high clouds moved in. Air temperature did not rise above 0°C.

Table A16. Physical Parameters of Snow Cover 24 February 1978

LAYER	GRAIN TYPE	GRAIN SIZE (mm)	DENSITY (g/cm^3)	HEIGHT (cm)	TEMPERATURE DEG C (0, −5, −10, −15)	COMMENTS
				80		Average surface hardness: 5000 g/cm^2.
Crust	Rounded	1				NOTE ON SURFACE CRUST: Most grains bonded together. Average size is 2mm. Some are as large as 3 mm.
Snow of 3 Feb.	Rounded	1	0.22	70		BELOW SURFACE: Grains are loosely bonded if bonded at all.
				60		Day was overcast and calm. Air temperature remained below 0°C during scattering measurements. High temperature of day was 1°C.
				50		
				40		
			0.50	30		
Snow of 20 Jan.				20		
18 Jan. and earlier snow				10		
				0		

Table A17. Physical Parameters of Snow Cover of 27 February 1978

LAYER	GRAIN TYPE	GRAIN SIZE (mm)	DENSITY (g/cm^3)	HEIGHT (cm)	TEMPERATURE DEG C	COMMENTS
					0 −5 −10 −15	
				80		Average surface hardness: 5333 g/cm^2.
Crust	Rounded	1				Snow crust and snow below crust unchanged from observation of 24 February.
Snow of 6 Feb.	Rounded	1	0.23	70		Day was sunny and calm. Air temperature did not rise above 0°C.
				60		
				50		
			0.29	40		
				30		
Snow of 20 Jan.				20		
18 Jan. and earlier snow				10		
				0		

Table A18. Physical Parameters of Snow Cover 28 February 1978

LAYER	GRAIN TYPE	GRAIN SIZE (mm)	DENSITY (g/cm^3)	COMMENTS
Crust	Rounded	1		Average surface hardness: 5353 g/cm².
Snow of 6 Feb.	Rounded	1	0.25 0.32	Structure of snow below crust unchanged from observation of 24 February.
Snow of 20 Jan.				Day [illegible] Air temperature did not rise above -2°C.
18 Jan. and earlier snow				

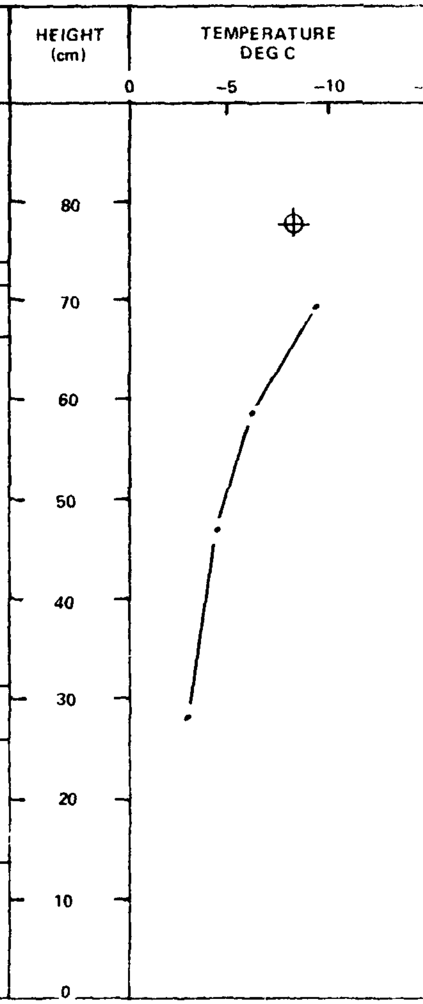

Table A19. Physical Parameters of Snow Cover 1 March 1978

LAYER	GRAIN TYPE	GRAIN SIZE (mm)	DENSITY (g/cm^3)	HEIGHT (cm)	TEMPERATURE DEG C (0, -5, -10, -15)	COMMENTS
				80		Average surface hardness: 5333 g/cm^2.
Crust	Rounded	1				
Snow of 6 Feb.	Rounded	1	0.29	70		Grains were bonded together to form particles as large as 5 mm. Otherwise no change from 24 February.
				60		*Morning* was partially overcast and calm. Afternoon was clear and calm. Air temperature did not exceed -4°C.
				50		
				40		
			0.32	30		
Snow of 20 Jan.				20		
18 Jan. and earlier snow				10		
				0		

Table A20. Physical Parameters of Snow Cover 2 March 1978

LAYER	GRAIN TYPE	GRAIN SIZE (mm)	DENSITY (g/cm^3)	HEIGHT (cm)	TEMPERATURE DEG C (0, -5, -10, -15)	COMMENTS
				80		Average surface hardness: 5333 g/cm^2.
Crust	Rounded	1				
Snow of 6 Feb.	Rounded	1	0.27	70		Snow crust and snow below crust unchanged from observation of 24 February.
				60		Day was clear and calm in morning, somewhat windy in afternoon. Air temperature did not rise above -5°C.
				50		
			0.35	40		
				30		
Snow of 20 Jan.				20		
18 Jan. and earlier snow				10		
				0		

MISSION
of
Rome Air Development Center

RADC plans and executes research, development, test and selected acquisition programs in support of Command, Control Communications and Intelligence (C^3I) activities. Technical and engineering support within areas of technical competence is provided to ESD Program Offices (POs) and other ESD elements. The principal technical mission areas are communications, electromagnetic guidance and control, surveillance of ground and aerospace objects, intelligence data collection and handling, information system technology, ionospheric propagation, solid state sciences, microwave physics and electronic reliability, maintainability and compatibility.

Printed by
United States Air Force
Hanscom AFB, Mass. 01731


DATE
ILME